

RESEARCH ARTICLE

Open Access



Comparative whole-genome transcriptome analysis in renal cell populations reveals high tissue specificity of MAPK/ERK targets in embryonic kidney

Kristen Kurtzeborn^{1,2†}, Hyuk Nam Kwon^{1,2†}, Vladislav Iaroshenko^{1,2}, Imrul Faisal^{1,2,3}, Martin Ambrož⁴, Xing Jin⁵, Talha Qureshi^{1,2}, Jussi Kupari^{1,6}, Anneliis Ihermann-Hella^{1,2}, Juho Väänänen⁷, Henna Tynyismaa^{2,8,9}, Iva Boušová⁴, Sunghyounk Park⁵ and Satu Kuure^{1,2,10*} 

Abstract

Background: MAPK/ERK signaling is a well-known mediator of extracellular stimuli controlling intracellular responses to growth factors and mechanical cues. The critical requirement of MAPK/ERK signaling for embryonic stem cell maintenance is demonstrated, but specific functions in progenitor regulation during embryonic development, and in particular kidney development remain largely unexplored. We previously demonstrated MAPK/ERK signaling as a key regulator of kidney growth through branching morphogenesis and normal nephrogenesis where it also regulates progenitor expansion. Here, we performed RNA sequencing-based whole-genome expression analysis to identify transcriptional MAPK/ERK targets in two distinct renal populations: the ureteric bud epithelium and the nephron progenitors.

Results: Our analysis revealed a large number (5053) of differentially expressed genes (DEGs) in nephron progenitors and significantly less (1004) in ureteric bud epithelium, reflecting likely heterogeneity of cell types. The data analysis identified high tissue-specificity, as only a fraction (362) of MAPK/ERK targets are shared between the two tissues. Tissue-specific MAPK/ERK targets participate in the regulation of mitochondrial energy metabolism in nephron progenitors, which fail to maintain normal mitochondria numbers in the MAPK/ERK-deficient tissue. In the ureteric bud epithelium, a dramatic decline in progenitor-specific gene expression was detected with a simultaneous increase in differentiation-associated genes, which was not observed in nephron progenitors. Our experiments in the genetic model of MAPK/ERK deficiency provide evidence that MAPK/ERK signaling in the ureteric bud maintains epithelial cells in an undifferentiated state. Interestingly, the transcriptional targets shared between the two tissues studied are over-represented by histone genes, suggesting that MAPK/ERK signaling regulates cell cycle progression and stem cell maintenance through chromosome condensation and nucleosome assembly.

Conclusions: Using tissue-specific MAPK/ERK inactivation and RNA sequencing in combination with experimentation in embryonic kidneys, we demonstrate here that MAPK/ERK signaling maintains ureteric bud tip cells, suggesting

[†]Kristen Kurtzeborn and Hyuk Nam Kwon are co-first authors.

*Correspondence: satu.kuure@helsinki.fi

¹⁰ GM-unit, Laboratory Animal Center, Helsinki Institute of Life Science, University of Helsinki, Helsinki, Finland

Full list of author information is available at the end of the article



a regulatory role in collecting duct progenitors. We additionally deliver new mechanistic information on how MAPK/ERK signaling regulates progenitor maintenance through its effects on chromatin accessibility and energy metabolism.

Background

Mitogen-activated protein kinase/extracellular signal-regulated kinase (MAPK/ERK) is best known for its function in regulating cellular proliferation and cell cycle progression [1]. The kinase cascade leading to MEK-induced phosphorylation of ERK in normal cells is typically induced by an extracellular stimulus conveyed by growth factors and other extracellular stimuli [2]. Activation of ERK kinases leads to both transcriptional regulation of target genes and phosphorylation of cytosolic substrates [3–5]. The vast majority of MAPK/ERK functions have been identified in different cancer types, while its significant roles in morphogenesis are emerging [6–9]. Our recent work suggests that MAPK/ERK signaling is also an important regulator of kidney development [10].

Kidney development is a complex process guided by the inductive interactions and mediated by inter- and intra-cellular signaling cascades. These interactions mainly take place between and among epithelial ureteric bud (UB) tips and the metanephric mesenchyme (MM) but also receiving contributions from the stroma [11–14]. In particular, receptor tyrosine kinase (RTK)-activated signaling, induced by glial cell line-derived neurotrophic factor (GDNF)/RET and fibroblast growth factors (FGFs), plays crucial roles in regulating nephrogenesis and UB branching morphogenesis, through which the embryonic kidney grows in size and achieves its typical shape [15, 16]. Each newly formed UB tip is responsible for maintaining most of the SIX2+ nephron progenitor cells within the MM population [17–19]. Simultaneously, together with stromal signals, the UB induces MM subpopulation to undergo a stepwise mesenchymal-to-epithelial transformation and in this way ensures their timely maintenance/differentiation balance [11, 20, 21].

The embryonic kidney hosts progenitor populations that are lost either during development or soon after birth [20]. Nephron progenitors represent a heterogeneous population with differences in their cell cycle length, motility, and molecular profiles [22–26], but the causes and purpose of such variation remain obscure. The UB epithelium on the other hand is molecularly and cellularly divided into UB tips and UB stalks, which have distinct transcriptional profiles and developmental programs; the tips execute branching morphogenesis by bifurcation while differentiation takes place in

the stalks [27–32]. The tips of the UB contain the progenitor cells for the entire collecting duct network, which allows fluid transport and urine excretion in the functional organ [33–36].

We and others have shown that the MAPK/ERK pathway is heterogeneously activated in several tissue types in the early developing kidney [37–39], and our recent live-imaging analysis revealed the highest activity in the UB tip cells, nephron progenitors, and differentiating nephron precursors [40]. Our previous work shows that tissue-specific knockout of MAPK/ERK in either UB or MM results in severe renal hypodysplasia through distinct mechanisms [10]. The lack of MAPK/ERK activity specifically in the UB epithelium results in thin tips which fail to change growth direction and give rise to a non-complex, oversimplified UB tree due to defective cell cycle progression, and cell-cell as well as cell-to-matrix adhesions [39]. In the MM, dynamic MAPK/ERK activation is needed for the maintenance of nephron progenitor identity through its functions in regulating the integrity of the nephrogenic niche [40].

In this study, we performed two RNA sequencing (RNA-Seq) experiments to identify transcriptional MAPK/ERK targets that participate in mediating its functions in the developing kidney. With the help of tissue-specific *Mek1/2* inactivation, green fluorescent protein (GFP) expression, and fluorescence-activated cell sorting (FACS) purification, we have identified specific targets for both the ureteric bud and nephron progenitor populations of the developing kidney but also revealed that a minor fraction of targets are shared. Our experimental data demonstrate for the first time that MAPK/ERK activation maintains the UB tip cells and participates in the prevention of its premature differentiation. Furthermore, the identified targets indicate mitochondrial metabolism as one of the key mechanisms through which MAPK/ERK activity regulates the nephron progenitors.

Results

Identification of transcriptional MAPK/ERK targets in renal progenitor populations

We have previously demonstrated that MAPK/ERK signaling is tissue-specifically regulating UB morphogenesis and the maintenance and differentiation of the MM [39, 40]. However, the transcriptional regulation through which MAPK/ERK functions in these tissues remains unknown. To investigate this, we utilized two different

mouse models to perform RNA-Seq on UB epithelial and MM cells. To facilitate the identification of primary rather than secondary MAPK/ERK targets, the RNA was isolated from tissues at the stages where the activity of the MAPK/ERK pathway was firstly mainly depleted and morphological defects only emerging. Based on our previous characterization of the renal phenotypes in these models [39, 40], E12.5 kidneys were used for isolation of control and MAPK-deficient UB (UB_{dko}; HoxB7CreGFP; Mek1^{fl/fl}; Mek2^{-/-}) and E13.5 kidneys for control and MAPK-deficient MM (MM_{dko}; Six2-TGC^{tg/+}; Mek1^{fl/fl}; Mek2^{-/-}) populations (Fig. 1A, B) ($n = 2$ kidneys per sample, four and three biological replicates per genotype, respectively). Principal component analysis (PCA) showed that control and *Mek1/2* double-knockout (dko) samples cluster well within their own populations but are clearly distinct from each other (Additional file 1: Fig. S1). Gene expression levels of the dko populations were normalized against the control populations, and differential expression analysis between each wildtype and UB_{dko}/MM_{dko} was performed through R/Bioconductor package DESeq2 [41].

RNA-Seq identified 55,335 transcripts in the UB and 52,636 transcripts in the MM (Fig. 1C). To reveal RNAs enriched in MAPK/ERK-deficient UB and MM cells, the transcripts were filtered using a statistical cutoff of $P_{\text{adj}} < 0.05$ and a magnitude threshold of $|\log_2\text{foldchange}| \geq 1$. As a result, 1004 significantly differentially expressed genes (DEGs) were identified in the UB epithelium and 5053 in the MM (Fig. 1C, Additional file 2: Table S1 and Additional file 3: Tables S2). The high number of DEGs especially in MM probably reflects its cellular heterogeneity, which is also detected to a lesser extent in the UB [26, 30, 42–45]. Of our dataset, 63% of DEGs in the UB_{dko} are upregulated (632) and 37% downregulated (372),

while DEGs in the MM_{dko} dataset are more evenly distributed and comprised 46% upregulated (2341) and 54% downregulated (2713) genes (Fig. 1D–F).

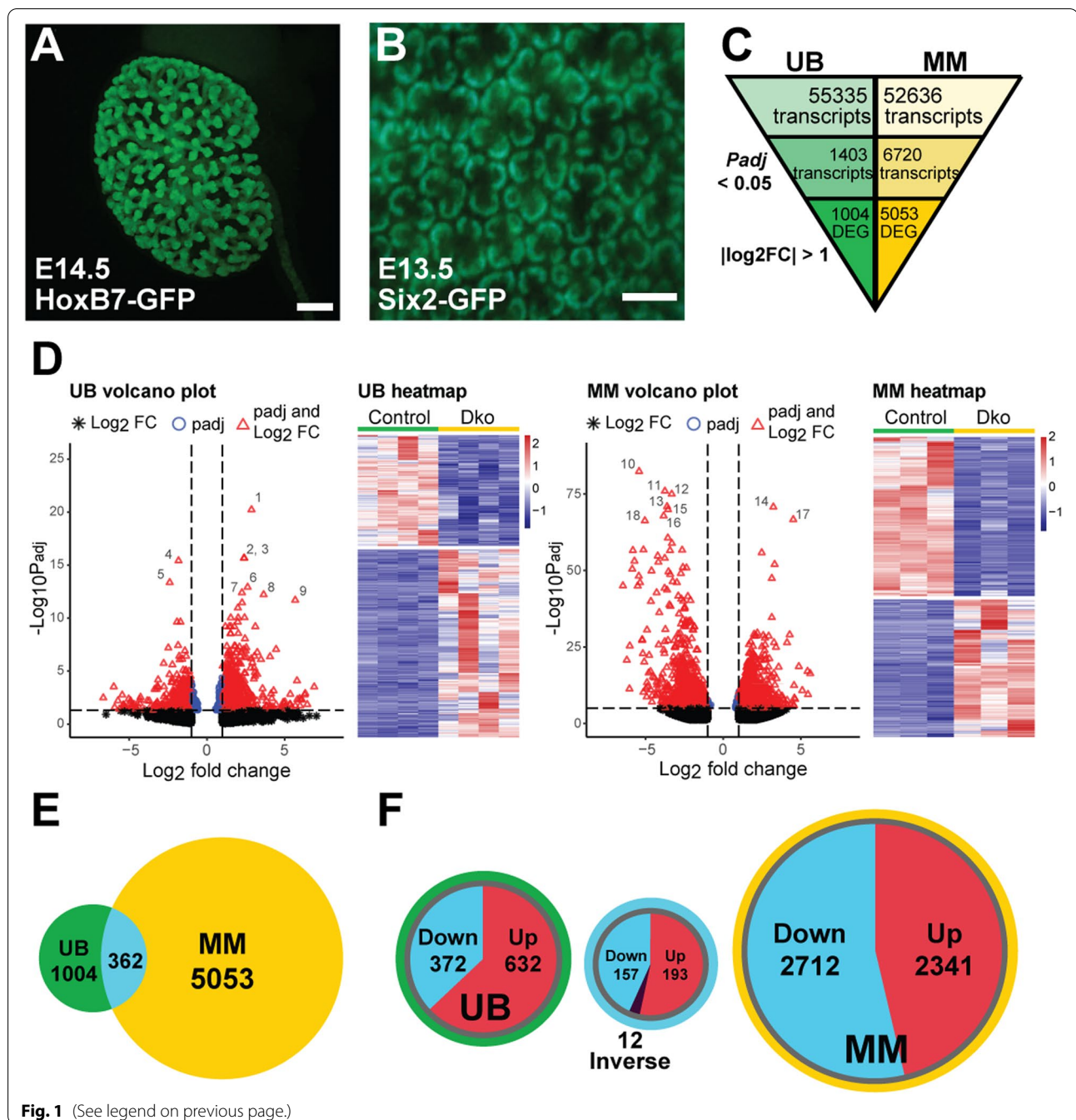
Analysis of the MAPK/ERK transcriptomes reveals high tissue-specific fidelity

To characterize the gene expression changes in each tissue at a general level, a Gene Ontology (GO) analysis of the DEGs of UB_{dko} and MM_{dko} cells was performed. This identified significant ($P_{\text{adj}} < 0.05$) alteration of 595 (UB) and 1035 (MM) biological processes, 80 (UB) and 257 (MM) cellular components, and 29 (UB) and 144 (MM) molecular functions, suggesting multifaceted roles for the MAPK/ERK cascade in both tissues of the developing kidney (Additional file 4: Table S3). In the UB, many of the DEGs are involved with cell motility, proliferation, response to stimuli, and epithelium development (Fig. 2). These changes are in line with, and substantiated by, the identified molecular changes and branching morphogenesis defect we previously reported for MAPK/ERK-deficient UBs [39].

In the MM, the most affected biological processes relate to cell cycle, intracellular protein transport, metabolism, and protein localization (Fig. 3). GO analysis of molecular functions in both cell types revealed changes related to enzymatic activities, such as transferases and kinases but also identified distinct functions in DNA- (UB_{dko}) and RNA- (MM_{dko}) binding and ribonucleotide biology, including purine binding (MM_{dko}) (Additional file 1: Fig. S2A–B). Cellular component analysis further confirmed the cell type-specific changes caused by MAPK/ERK deficiency and additionally revealed UB-specific transcriptional alterations that relate to organelle structures including membranes, Golgi apparatus, cell junctions, and endosomes, while in the MM, a remarkable amount

(See figure on next page.)

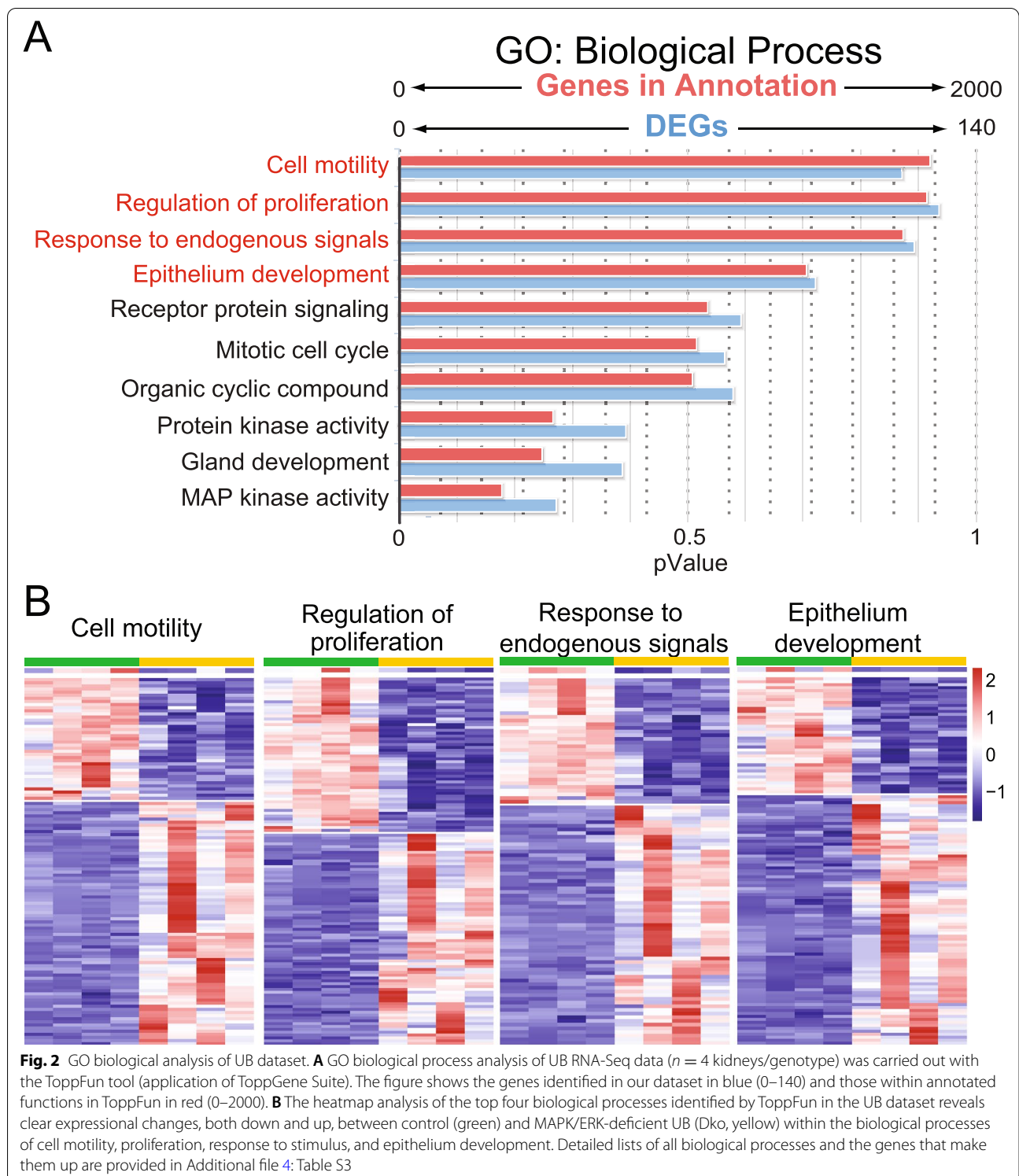
Fig. 1 Tissue-specific bulk RNA sequencing of MAPK/ERK-deficient renal progenitor populations. **A** Whole mount image example of a mouse kidney expressing HoxB7Cre-GFP in the ureteric bud (UB) epithelium and collecting ducts at E14.5. White scale bar represents 300 μm . **B** Example whole mount image of the cortical surface of a mouse kidney expressing Six2-TGC-GFP in the nephron progenitor/metanephric mesenchyme (MM) population at E13.5. White scale bar represents 150 μm . **C** RNA-Seq was separately performed on E12.5 control ($n = 4$ kidneys) and MAPK/ERK-deficient UB (*HoxB7Cre-GFP; Mek1^{fl/fl}; Mek2^{-/-}*, $n = 4$ kidneys) and E13.5 control ($n = 3$ kidneys) and MAPK/ERK-deficient nephron progenitors (*Six2-TGC-GFP; Mek1^{fl/fl}; Mek2^{-/-}*; $n = 3$ kidneys). Among the total reads of 55,335 and 52,636 in UB and MM, respectively, 1403 genes in the UB and 6720 in the MM were identified to be significantly differentially expressed with a cutoff of $P_{\text{adj}} < 0.05$. Further filtering with $|\log_2\text{fold change}| \geq 1$ revealed 1004 differentially expressed genes (DEGs) for UB and 5053 for MM. **D** Volcano plot and heatmap for DEGs between wildtype and dko populations in the UB (left). Similar to the UB, the volcano plot and heatmap for MM (right) demonstrate clear segregation of the control samples from those lacking MAPK/ERK (dko) activity in UB and MM populations. The most prominent DEGs are numbered in the plots and represent the following genes: 1, *Ccdc141*; 2, *Igfbp5*; 3, *Slc40a1*; 4, *Ccnd1*; 5, *Etv5*; 6, *Atp2b4*; 7, *Samd9l*; 8, *Scn3b*; 9, *Xkr4*; 10, *Hist1h3c*; 11, *Rpl19*; 12, *Hist1h1a*; 13, *Rpl41*; 14, *mt-Rnr2*; 15, *Rpsa*; 16, *Rpl8*; 17, *Gm28439*; and 18, *Hist1h4d*. Significant DEGs in the volcano plots are marked as red dots with a statistical cutoff of $P_{\text{adj}} < 0.05$ and a magnitude threshold of $|\log_2\text{fold change}| \geq 1$. Heatmaps show downregulated genes in blue and upregulated genes in red; color intensity corresponds to the degree of differential expression. **E** Venn diagram shows 362 shared genes with differentially regulated expression in both UB and MM datasets. **F** Venn diagrams depicting up-/downregulated DEGs in UB and MM populations. Among the 1004 UB DEGs, we identified 372 genes (37%) whose expression was downregulated and 632 genes (63%) which were upregulated. Among the 362 shared DEGs between UB and MM, 157 genes (43%) were downregulated, and 193 genes (53%) were upregulated. Interestingly, 12 genes (3%) were inversely expressed, with six genes upregulated and six genes downregulated. Out of 5053 MM DEGs, 2712 genes (54%) were downregulated, and 2341 genes (46%) were upregulated



of DEGs related to mitochondria, catalytic complexes, and anchoring and adherens junctions (Additional file 1: Fig. S2C-D).

Finally, we analyzed how conserved are the MAPK/ERK transcriptional targets identified by RNA-Seq in UB and MM tissues of the developing kidney. A comparison of the two datasets to one another revealed 362 shared genes (36% and 7% of DEGs in UB and MM

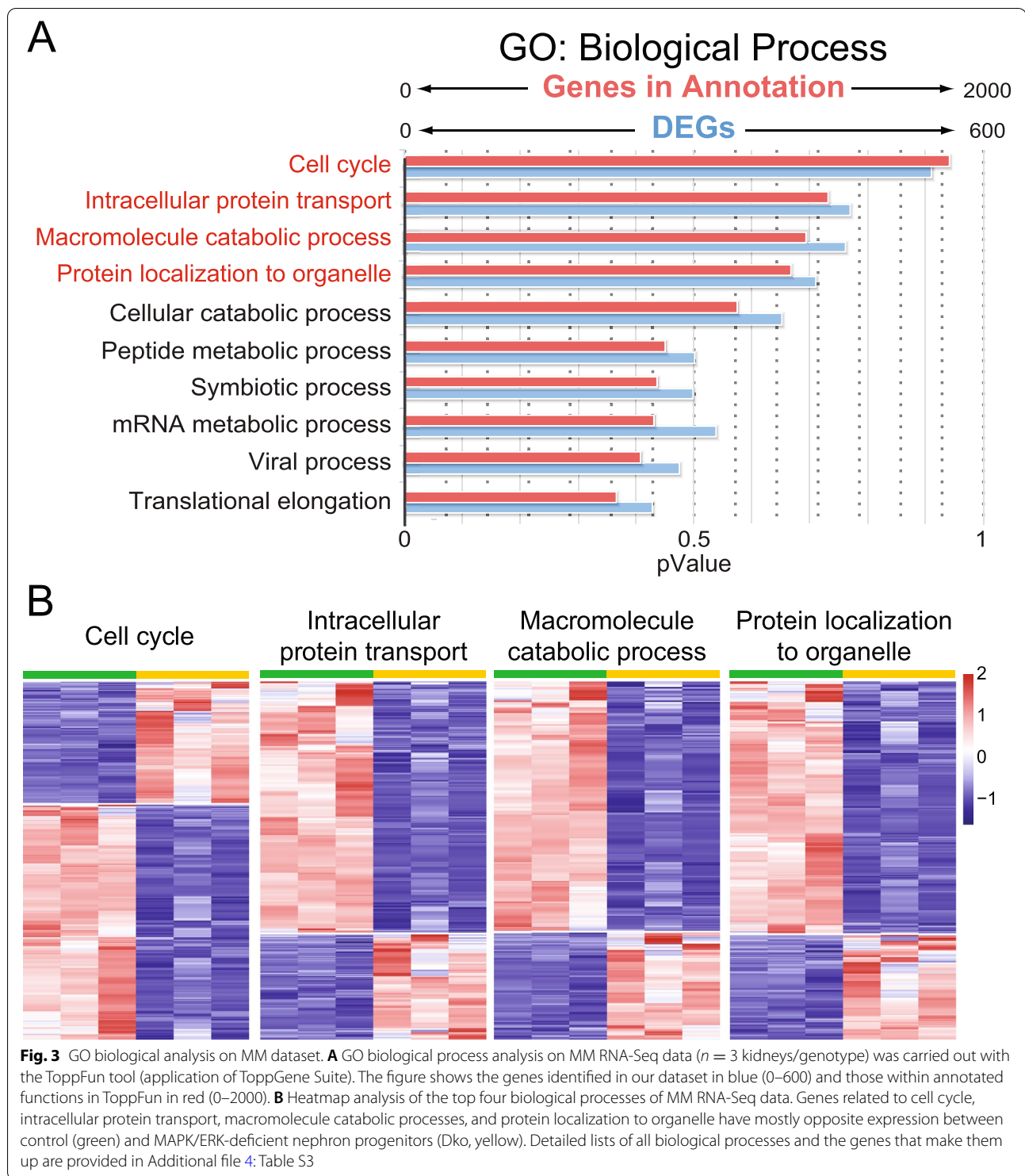
datasets, respectively), whose expression is changed in both tissues (Fig. 1E; Additional file 5: Table S4). This suggests that the majority of the gene expression changes caused by the MAPK/ERK pathway especially in the MM of developing kidney are highly tissue-specific, as 93% of the transcriptional changes in the MM and 64% in the UB take place only in the analyzed tissue but not in the other cell type of the developing kidney.



Shared UB and MM DEGs reflect epigenetic changes and suggest MAPK/ERK functions on histones and DNA methylation

Detailed analysis of the genes whose expression is

changed by MAPK/ERK inactivation in both UB and MM cells identified 53% upregulated transcripts (193), 43% downregulated transcripts (157), and only 12 genes (3%) which showed inverse differential expression



(Figs. 1F and 4A). The inverse DEG group is composed of 11 genes with confirmed protein-coding activity (Additional file 5: Table S4). Among these, *Sprouty 1* (*Spry1*), downregulated in UB_{dko} and upregulated in MM_{dko} , and *Cavin1*, downregulated in MM_{dko} and

upregulated in UB_{dko} , are known to inhibit MAPK/ERK signaling [46, 47] and have crucial roles in kidney development, along with *cadherin 6* and *Sox9* [48–52], also showing inverse expression in UB_{dko} and MM_{dko} (Additional file 5: Table S4).

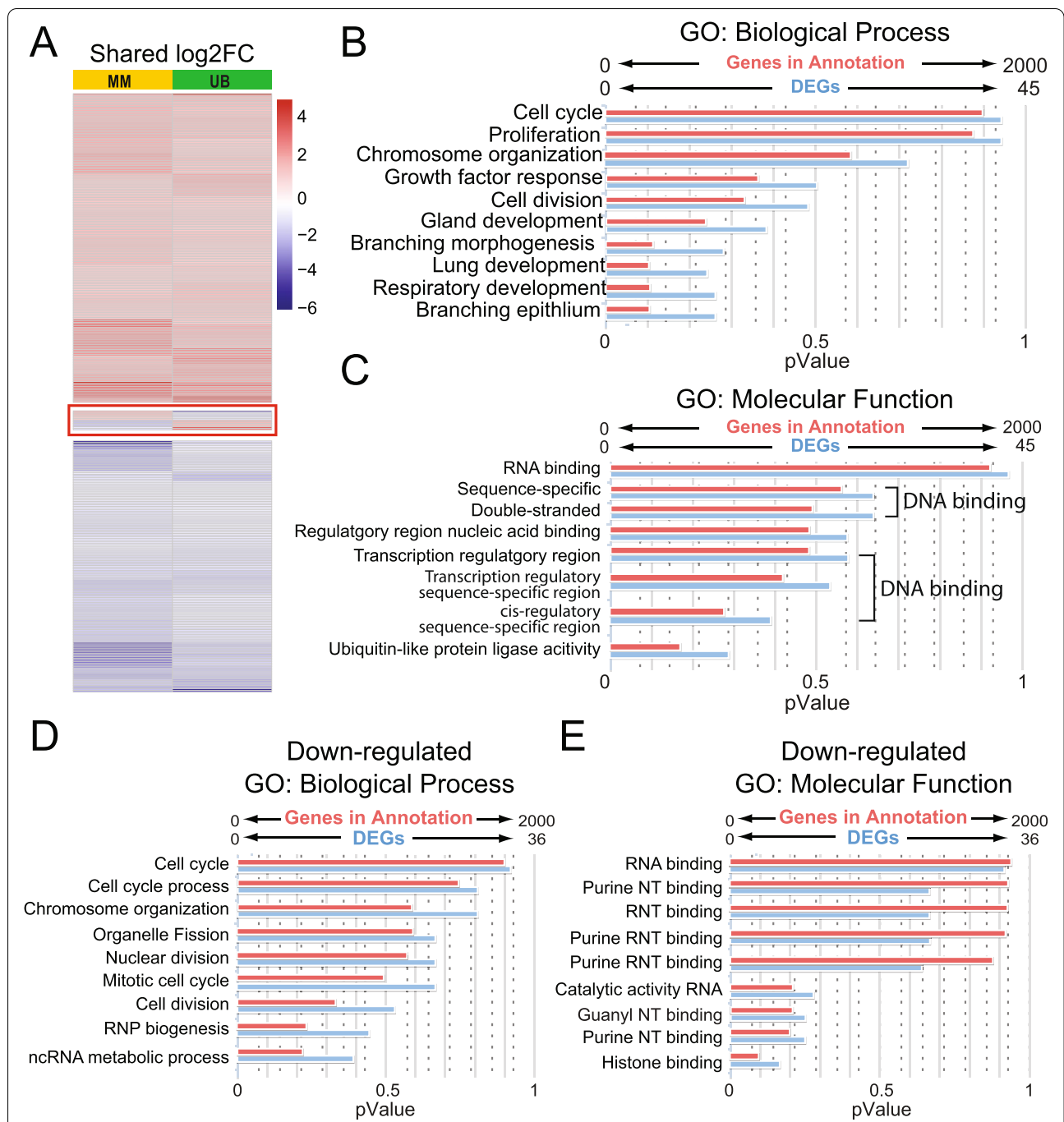


Fig. 4 Collecting duct and nephron progenitors share a minor pool of genes whose expression is regulated by MAPK/ERK in both tissues. **A** Heatmap analysis of 362 shared genes in UB and MM. Twelve inversely expressed genes are shown in the middle of the heatmap. **B** Gene Ontology (GO) biological process analysis of shared genes between UB and MM. **C** GO molecular function analysis of shared genes between UB and MM. **D** GO biological process analysis of downregulated shared genes. **E** GO molecular function analysis of downregulated shared genes. Blue bars represent input DEGs from our RNA-Seq, and red bars represent genes in annotation. Abbreviations: ncRNA; non-coding ribonucleic acid, NT; nucleotide, RNP; ribonucleoprotein, RNT; ribonucleotide. Detailed lists of all biological processes and the genes that make them up are provided in Additional file 6: Table S5

As expected from the previously known MAPK/ERK functions [3, 53], most of the shared MAPK/ERK targets encode proteins with functions related to cell cycle,

proliferation, response to growth factor, organ development, branching morphogenesis, and DNA/RNA binding (Fig. 4B, C, Additional file 6: Table S5). Among the 362

shared genes, GO analysis of the 193 upregulated DEGs revealed very few genes falling into any specific biological or molecular process category, thus demonstrating great diversity among upregulated DEGs that represent MAPK/ERK targets (Additional file 6: Table S5). On the other hand, GO analysis of the 157 downregulated shared genes reflects well with the biological processes and molecular functions identified within the total shared genes (Fig. 4D, E, compare to Fig. 4B, C). This suggests a strong and possibly universal regulatory function of MAPK/ERK cascade in processes such as cell cycle, proliferation, response to growth factor, organ development, and DNA/RNA binding.

The largest portion (13%) of the shared downregulated DEGs represent histones (Additional file 5: Table S4), and their GO analysis identified chromosome condensation and nucleosome assembly as the most affected biological processes (Additional file 6: Table S5). Indeed, 25 genes coding for histone cluster components, histone chaperones, or histone-associated kinases are downregulated in UB_{dko}, and a total of 69 histone-related genes are differentially expressed in MM_{dko} (Additional file 7: Table S6). Interestingly, the most downregulated gene in each dataset is a histone cluster gene, *Hist1h2br* (H2B clustered histone 24) in UB_{dko} and *Hist1h2ai* (H2A clustered histone 13) in MM_{dko}. In the MM_{dko}, 57 DEGs encoding histone cluster components were downregulated, of which 28 genes showed at least a 16-fold difference and occupied a place in the top 50 downregulated genes list, suggesting a major defect. Of note, *Dnmt1*, the gene coding for the DNA (cytosine-5)-methyltransferase 1 enzyme, which is responsible for most of the DNA methylation in mouse cells, is downregulated by twofold in both MAPK/ERK-deficient UB and MM (Additional file 5: Table S4), and *Dot1l* encoding histone H3 methyltransferase is significantly downregulated in MM_{dko} cells (Additional file 3: Table S2).

Finally, we wanted to test how universally the MAPK/ERK cascade regulates the genes identified by our RNA-Seq analysis. Quantitative PCR of 20 DEGs, selected based on their high DE scores and known importance in signal transduction and/or kidney development, was first carried out in whole E12.5 kidneys cultured in control and MAPK/ERK inhibition conditions. This showed that *Ccdc69*, *Cited2*, *Cpne7*, *Dusp6*, *Etv4*, *Fjx1*, *Flrt3*, *Fosb*, *Hist1h4k*, *Hist2h3b*, *Lypla1*, *Mfng*, *Trim12a*, and genes encoding proteins related to negative regulation of ERK (*Dusp6*) and with known roles during kidney development (*Etv4*) [54–56] are significantly differentially regulated in the MAPK/ERK-deficient whole kidneys ($P < 0.05$; Additional file 1: Fig. S3A). Analysis of specific gene expressions related to chromatin regulation (*Dnmt1*, *Hist1h2br*), cell growth (*Ppan*), tip identity (*Wnt11*),

cellular metabolism (*Acot7*, *Adsl*), and RTK signaling targets (*Wnt11*, *Etv4*) in isolated UB and MM populations confirmed the DEGs identified in RNA-seq (Additional file 1: Fig. S3B,C).

We also expanded our analysis of MAPK/ERK target expression to MAPK/ERK-inhibited embryonic lung and adult liver. We were able to detect that the shared transcriptional changes in DNA methyltransferase *Dnmt1*; carbohydrate derivative metabolism regulators *Acot7*, *Adsl*, and *Cad*; mitochondrial *Qtrt1*; RNA polymerase *Polr1e*; kinesin family member *Kifc1*; NME/NM23 nucleoside diphosphate kinase *Nme2*; and histone cluster gene *Hist1h2br* identified by RNA-Seq were recapitulated in the embryonic lung but not in adult liver (Additional file 8: Table S7).

MAPK/ERK activation in the ureteric bud is required to maintain tip cell identity

Next, we focused on tissue-specific transcriptional changes caused by MAPK/ERK deficiency in the UB. It has been established that UB tips host collecting duct progenitors capable of differentiating into mature collecting duct cell types [34, 35, 54, 55]. Rutledge et al. [30] previously reported segregation between genes enriched in UB tips and stalks and identified 116 tip-enriched and 393 stalk-enriched genes in E16.5 kidneys. We compared our DEGs in MAPK/ERK-deficient UB epithelium to their published tip- and stalk-enriched lists to reveal that the UB_{dko} dataset contains 39 transcripts previously identified as tip-enriched genes and 82 transcripts identified as stalk-enriched genes (Table 1).

Interestingly, all (100%) the genes previously classified as tip-enriched and found in our dataset (39/39) are downregulated, including the most highly enriched tip gene *Wnt11* identified by Rutledge et al. [30] (Table 2, Fig. 5A, Additional file 1: Fig. S3B). On the contrary, almost all (95%) previously identified UB stalk-enriched genes are upregulated in MAPK/ERK-deficient UBs (78/82). At the individual gene level, 18 genes out of 39 total genes have known functions in kidney development and are downregulated in UB_{dko} including well-characterized *Etv4*, *Etv5*, *Frem2*, *Gfra1*, *Ret*, and *Spred2* with central roles in UB morphogenesis (Table 2). The upregulated stalk-enriched genes include *Aqp4*, *Cav1*, *Krt7*, *Shh*, and *Serpinb9* with previously reported involvement in kidney development [74–78]. Interestingly, such a dramatic change in the tip-stalk gene expression pattern suggests that MAPK/ERK activity functions to maintain the progenitor status of the progenitor cells within the UB tip niche.

To further examine the underlying gene regulatory networks involved in UB tip identity, we next utilized the web-based StemChecker [79], which compares an

Table 1 Transcriptional changes with known tip-stalk localization identified in MAPK/ERK-deficient ureteric bud

UB-stalk-enriched genes upregulated in <i>Mek1/2</i> dko	Log2FC			UB-tip-enriched genes downregulated in <i>Mek1/2</i> dko	Log2FC
Atp6v0d2	5.82017	Paqr5	2.02776	Stmn1	-1.0135
Thrb	5.68810	Neat1	1.99209	Rprm	-1.0289
Vsig1	4.44785	Cpeb2	1.94871	Frem2	-1.0412
Trim47	4.07919	Dab2	1.93896	Ctnnd2	-1.0942
Serpinb9	3.74231	Ppp1r3c	1.90854	Uhrf1	-1.1082
Tmem117	3.59284	Itpr2	1.88864	Stra6	-1.1199
Wdr72	3.58091	Akr1c19	1.86199	Gfra1	-1.1478
Trim16	3.24198	Pdlim1	1.84855	Sema6a	-1.1662
Tspan8	3.23112	Scnn1a	1.83277	Kdm2b	-1.1890
Igf1	3.05885	Nr3c1	1.82302	Mycn	-1.2976
Cav1	3.04600	Igfbp7	1.72571	Slc27a6	-1.3305
Muc20	3.02456	Elf5	1.69912	Fbln1	-1.3432
Ccdc141	2.86843	Prlr	1.69734	Ung	-1.3621
Tmem45b	2.86742	Scnn1b	1.68607	Dctd	-1.3629
Gsta3	2.85412	Bmp3	1.67283	Sox8	-1.4139
Nipal1	2.82231	Lypd6	1.63446	Nsg1	-1.4406
Rhcg	2.80980	Slc29a1	1.63091	Cdca7	-1.4578
Ugt2b34	2.69559	Ampd3	1.63017	Hs3st3b1	-1.4741
Krt80	2.63243	Reps2	1.62458	Spred2	-1.4753
Cers3	2.57988	Fam13a	1.57950	Acot7	-1.5284
Foxa1	2.46191	Plxna2	1.57511	Fxyd6	-1.5755
Anxa3	2.44622	Pde7b	1.53769	Fbln2	-1.5889
Pde1a	2.41531	Dkk3	1.53697	Tmem59l	-1.6118
Acpp	2.40222	Atp1b1	1.52502	Spry4	-1.6210
Slc40a1	2.37983	Meg3	1.46617	Ret	-1.7017
Slco2a1	2.36114	Foxq1	1.42632	Ror2	-1.7602
Emp1	2.34928	AA986860	1.41052	Adamts18	-1.8082
Fxyd4	2.22886	Parm1	1.34588	Ccnd1	-1.8272
Pdzk1	2.19846	Slc7a8	1.31827	Cxcl14	-1.9303
Cav2	2.14791	Itgb6	1.30563	Kank4	-1.9339
Efemp1	2.14526	Rcan2	1.28463	Mfsd2a	-1.9530
Shh	2.13946	Tmprss2	1.25556	Ak1	-1.9839
Pdzk1ip1	2.09042	Sparc	1.23359	Psmc3ip	-2.0363
Plcd1	2.08808	Krt7	1.20999	Etv4	-2.1504
Efcab1	2.08737	Eno2	1.20676	Wnt11	-2.1618
Aqp4	2.08663	Car12	1.19927	Psrc1	-2.2083
Nr3c2	2.04846	Bmf	1.12381	Etv5	-2.3936
1810019D21Rik	2.03767	Nedd4l	1.09804	Cib2	-2.8918
Atp10b	2.03048	Cystm1	1.02906	Nrtn	-5.3538

input gene list to those published for known transcription factor target gene sets. Using the DEGs from the UB RNA-Seq, we compared the enrichment of up- and downregulated genes among transcription factor target genes (Additional file 1: Fig. S4). Among the downregulated genes, we observed a significant overrepresentation of genes targeted by pluripotency master regulators *Oct4* and *Sox2* as well as proliferation regulators *Myc*, *Max*,

and *E2f4* [80–82]. In contrast, the results for upregulated genes revealed that they were the main targets of polycomb complex components *Ezh2*, *Suz12*, and *Ring1B* [83]. These findings provide additional evidence that MAPK-deficient UB tip cells lose their progenitor state and proliferative/self-renewal capacity while increased expression of genes targeted by polycomb complexes, which function to repress developmental regulatory

Table 2 Downregulated tip-enriched genes with known functions in kidney development. 19 out of 39 genes with previously characterized tip-specific expression pattern play well-known functions in ureteric bud morphogenesis and are cited in references column

Gene	References
<i>Nrtn</i>	Davies et al. [57]
<i>Etv5</i>	Lu et al. [54]; Kuure et al. [55]
<i>Wnt11</i>	Majumdar et al. [58], O'Brien et al. [59]
<i>Etv4</i>	Lu et al. [54]; Kuure et al. [55]
<i>Cxcl14</i>	Schmidt-Ott et al. [28]
<i>Ccnd1</i>	Ihermann-Hella et al. [39]
<i>Adamts18</i>	Rutledge et al. [60]
<i>Ror2</i>	Nishita et al. [61]
<i>Ret</i>	Schuchardt et al. [62]; reviewed in Costantini [63]
<i>Spry4</i>	Zhang et al. [64]
<i>Hs3st3b1</i>	Rutledge and McMahon [65]
<i>Sox8</i>	Reginensi et al. [50]
<i>Mycn</i>	Stanton et al. [66]; reviewed in Hohenstein et al. [67]; Pan et al. [68]
<i>Gfra1</i>	Cacalano et al. [69]; Enomoto et al. [70]; reviewed in Costantini [63]
<i>Ctnnd2</i>	Rutledge et al. [30]
<i>Frem2</i>	Jadeja, et al. [71]; Kiyozumi, et al. [72]
<i>Rprm</i>	Magella et al. [73]
<i>Stmn1</i>	Li et al. [30]

genes in mouse embryonic stem cells [84], further supports this.

To examine the transcriptome-suggested change in cell type fate in vivo, we analyzed the maturation status of MAPK/ERK-deficient UB epithelium at the protein level in embryonic kidneys. UB tips host collecting duct progenitors that give rise to the mature collecting duct epithelium with two main differentiated cell types, namely intercalated and principal cells [85, 86]. Immunofluorescence staining was performed with markers detecting principal (aquaporin 2 (AQP2), Na/K-ATPase) and intercalated (V-ATPaseB1/2) cells of the collecting duct (Fig. 5). In control kidneys at E16.5, AQP2 localized solely to the medullar principal cells, and V-ATPase was found in the medullar intercalated cells while, as expected, the cortical UB tips lack all three tested differentiation markers (Fig. 5C, E, G). Notably, all three tested markers, AQP2, V-ATPase, and Na/K-ATPase, were more abundantly detected in the UB_{dko} kidneys where they additionally localized to the cortical-most regions of ureteric buds representing the tip population (Fig. 5D, F, H). These results support our transcriptional findings and show that UB cells lacking

MAPK/ERK activity prematurely differentiate into mature collecting duct cell types. In conclusion, MAPK/ERK activity, through maintaining the UB tip identity, is essential for preventing premature differentiation of the UB epithelium.

MAPK/ERK activity regulates genes for mitochondrial functions in nephron progenitors

Our GO analysis of the MM dataset revealed that several interesting cellular components related to the mitochondria are differentially expressed upon MAPK/ERK inactivation (Additional file 1: Fig. S2D, Additional file 1: Fig. S3C). Further characterization of the MM dataset with mitochondria-related biological processes identified DEGs in MM_{dko} that involve processes of mitochondrial respiratory chain function (Fig. 6A). Because most of the transcripts related to mitochondrial functions appear downregulated in the MM_{dko} dataset (representing nephron progenitors), we wanted to distinguish between the possibilities of general mitochondria count versus mitochondrial functionality being affected by MAPK/ERK activity. The analysis of mitochondrial DNA (mtDNA) copy number in control and MAPK/ERK-deficient kidneys at E12.5 revealed that, indeed, mitochondria amount per cell, as determined by mtDNA copy number against nuclear DNA copy number, was statistically significantly reduced (Fig. 6B). This suggests that the MAPK/ERK pathway is required for the mitochondrial replenishment in actively dividing nephron progenitors.

Finally, we wanted to further examine the possibility that diminished mitochondria fail to fuel cells in the absence of MAPK/ERK activation, a hypothesis also supported by the finding that adenosine triphosphate (ATP)-related metabolic activity was one of the mitochondrial functions affected by MAPK/ERK deficiency (Fig. 6A). To test the functional capacity of the mitochondria upon MAPK/ERK inhibition, we measured the actual ATP amounts in embryonic kidney cells by using liquid chromatography–mass spectrometry (LC/MS). This analytic quantification revealed a significant decrease of ATP amount in MAPK/ERK-inhibited cells (Fig. 6C). In line with this, Seahorse analysis showed decreased ATP production and further indicated impaired basal respiration, maximal respiration, and spare capacity in MAPK/ERK-inhibited cells (Fig. 6D, E). Taken together, our RNA-Seq of MM_{dko} identified a decline in mitochondria-related biological processes, which are functionally supported by lower mtDNA copy number, oxygen consumption, and quantitative ATP level. Consequently, our observations suggest that MAPK/ERK deficiency in nephron progenitors leads

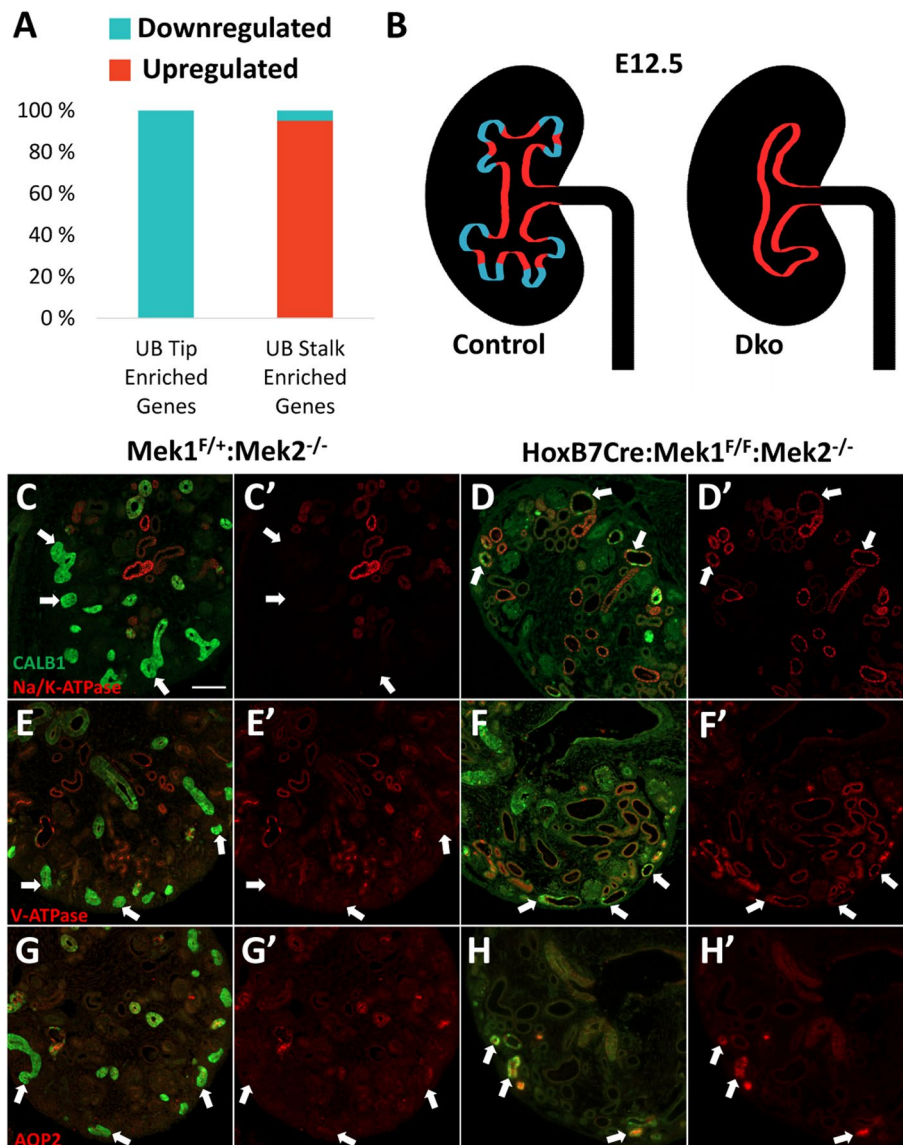


Fig. 5 MAPK/ERK-deficient UB tips prematurely differentiate into UB stalk-like cells. **A** Comparison of differentially expressed genes in UB_{dko} to a published dataset of genes with enriched expression in either the UB tip or UB stalk (Rutledge et al.) revealed that of the previously identified UB tip-enriched genes that are differentially expressed in the UB_{dko}, all (39/39 genes) are downregulated (blue). Of the UB stalk-enriched genes differentially expressed in the UB_{dko}, 95% (78/82 genes) are upregulated (red). **B** Schematic representation of the gene expression changes between the UBs of wildtype (control) and *HoxB7Cre-GFP;Mek1^{F/F};Mek2^{-/-}* (dko) kidneys at E12.5. It is known that the control kidney has distinct gene expression signatures in the UB tips (blue) compared to the UB stalks (red). Additionally, the control kidney exhibits a stereotypic branching pattern. We have shown previously that in the absence of MAPK/ERK activation, the UB has a noticeable branching defect. Our analysis here revealed that MAPK/ERK-deficient UB epithelium loses the expression of tip specific genes and instead shows upregulation of stalk-enriched genes ($n = 4$ kidneys/genotype). **C–H'** Immunofluorescent staining of the E16.5 kidney paraffin sections. Calbindin-1 (CALB1) labels UB epithelium (green), and arrows indicate CALB1-positive cortical UB epithelium. **C–D'** Na/K-ATPase (red), a marker of principal cells in the mature collecting duct, is absent in the cortical UB tips of **C, C'** control kidneys but is detected in CALB1-positive cortical UB epithelium in **D, D'** UB_{dko}. Similarly, V-ATPase-B1/2 (red), a marker of intercalated cells in the mature collecting duct, is absent in the cortical epithelium of **E, E'** control kidneys but localized to cortical epithelium of **F, F'** UB_{dko}. **G, G'** Aquaporin-2 (AQP2), another marker of intercalated cells, is also absent from control but **H, H'** detected in UB_{dko} cortical epithelium. Scale bar, 100 μ m

to mitochondrial defects, which possibly contribute to the defects in progenitor self-renewing and provide grounds for more in-depth follow-up studies.

Discussion

Although the importance of the MAPK/ERK signaling pathway in the early developing kidney has been

demonstrated by us and others [10, 27, 38, 87], the tissue-specific impacts of MAPK/ERK signals on transcriptional regulation are not fully understood. Moreover, MAPK/ERK activation in tissues of developing kidneys is highly dynamic [40], suggesting differences in cellular responses. The MAPK/ERK activation pattern has been intimately linked with the type of transcriptional response in the signaling cell, where dynamic activation typically results in more efficient transcription of target genes, which however are subject to heavy post-translational regulation [88]. In order to elucidate deep insights into the transcriptional MAPK/ERK targets at the genetic level, we here performed RNA-Seq on cells isolated from tissue-specific MAPK-deficient kidneys (UB_{dko} and MM_{dko}) which are composed of heterogenous progenitors. RNA-Seq was carried out at the earliest time point where we have previously verified the loss of MAPK/ERK activity but where the kidney size is not impacted [39, 40]. In this way, our aim was to identify the primary MAPK/ERK targets in the given tissue, though this strategy may miss transcripts affected by partial downregulation of the pathway activity and also capture secondary targets. Profiling at different developmental stages might provide more information, but due to complex genetics of conditional deletion of multiple genes requiring an excessive amount of breeding mice, it would be tedious, expensive, and contrary to 3R principles. Moreover, different ERK activation modes and strengths are now known to regulate distinct transcriptional outputs resulting in varied cell fate decisions [88–90]. The next strategy to take would be single-cell RNA-Seq profiling of ERK high and low activity cells in UB and MM [40, 91]. Comparison of targets identified with the help of Förster Resonance Energy Transfer (FRET)-biosensor visualization of activation strengths to the bulk RNA-Seq targets identified here will deliver more insight not only into progenitor heterogeneity but also to their MAPK/ERK dependence.

Gene expression profiles of whole wildtype kidneys at different developmental stages have been reported

through microarray analysis [92], but the complete lack of spatial definition of gene expression is a major limitation. Since the introduction of RNA-Seq [93], it has provided notable insights into early-stage renal development [45, 94]. Here, we provide the first tissue-specific MAPK/ERK deficiency genetic profiles for UB and MM in the early developing kidney. The results suggest that MAPK/ERK targets are highly tissue-specific regardless of the pathway's rather universal control of proliferation through histone availability, adhesion, and energy metabolism via regulation of metabolic enzyme expression (Fig. 7). Tissue-specific transcriptional responses identified here are not unexpected as not only different growth factors but also the nature of MAPK/ERK activation, whether dynamic or sustained, induces distinct target gene expression and cell-fate outcomes [88–90, 95, 96]. As MM and UB are regulated by somewhat overlapping but hierarchically different growth factor cues [97, 98] and we have earlier demonstrated both sustained and dynamic MAPK/ERK activation in developing kidney tissues [40], target gene tissue specificity is in line with their complex expressional control.

One of the first RNA-seq results revealed rather broad transcriptional heterogeneity in a seemingly uniform nephron progenitor compartment [45], and this has since then been confirmed by others [26, 43, 44]. Brunskill and co-workers identified a few DEGs that are interesting and possibly relevant for our results. They observed some cells, mainly located in the periphery of the nephron progenitor niche, that simultaneously expressed nephron progenitor marker *Six2* and stromal marker *FoxD1* [19, 99] suggesting multilineage capacity for some early nephron progenitor cells [45]. *Six2* was not significantly differentially expressed in MAPK/ERK-deficient nephron progenitor cells. However, of the ten highest elevated gene expression in the uninduced MM compared to induced MM identified by Brunskill, six were downregulated in our MM dataset (*Ctsh*, *Osr1*, five *Coq9* family members (3, 6, 7, 8a, and 8b), *Arf2* family member *Arf5*, *Cpxm1*, and

(See figure on next page.)

Fig. 6 Gene expression changes in MAPK/ERK-deficient nephron progenitors suggest defects in mitochondrial functions. **A** Further heatmap analysis on the MM dataset revealed that mitochondria-related biological processes are affected in the absence of MAPK/ERK activation. The identified genes are listed in Additional file 9: Table S8. **B** Mitochondrial DNA copy number analysis was performed on control (DMSO, $n = 9$) and MEK1/2-inhibited (U0126, $n = 9$) E12.5 kidneys by real-time PCR. Mitochondrial DNA was measured by the analysis of its *12S* expression against nuclear DNA quantification by *Rbm* expression. **C** Quantification of ATP from mK4 cell line derived from embryonic kidney mesenchyme by LC/MS ($n = 4$ replicates for each DMSO and U0126). ATP concentrations are normalized against total protein concentration (Additional file 10: Table S9). $**p < 5 \times 10^{-3}$, $***p < 5 \times 10^{-6}$. **D** Oxygen consumption rate (OCR) of mK4 cell line was measured by a Seahorse XF analyzer. For the OCR measuring, ATP synthase inhibitor (oligomycin), protonophore uncoupler (FCCP), and ETC inhibitors (rotenone and antimycin A) were added at the indicated points ($n = 4$ replicates for each DMSO and U0126). **E** Basal respiration, ATP production, proton leak, maximal respiration, and spare capacity measures are shown in different samples. Error bars represent standard deviation (S.D.). NT, non-treated mK4 cells; DMSO, DMSO-treated mK4 cells as a control; U0126, MEK inhibitor U0126-treated mK4 cells

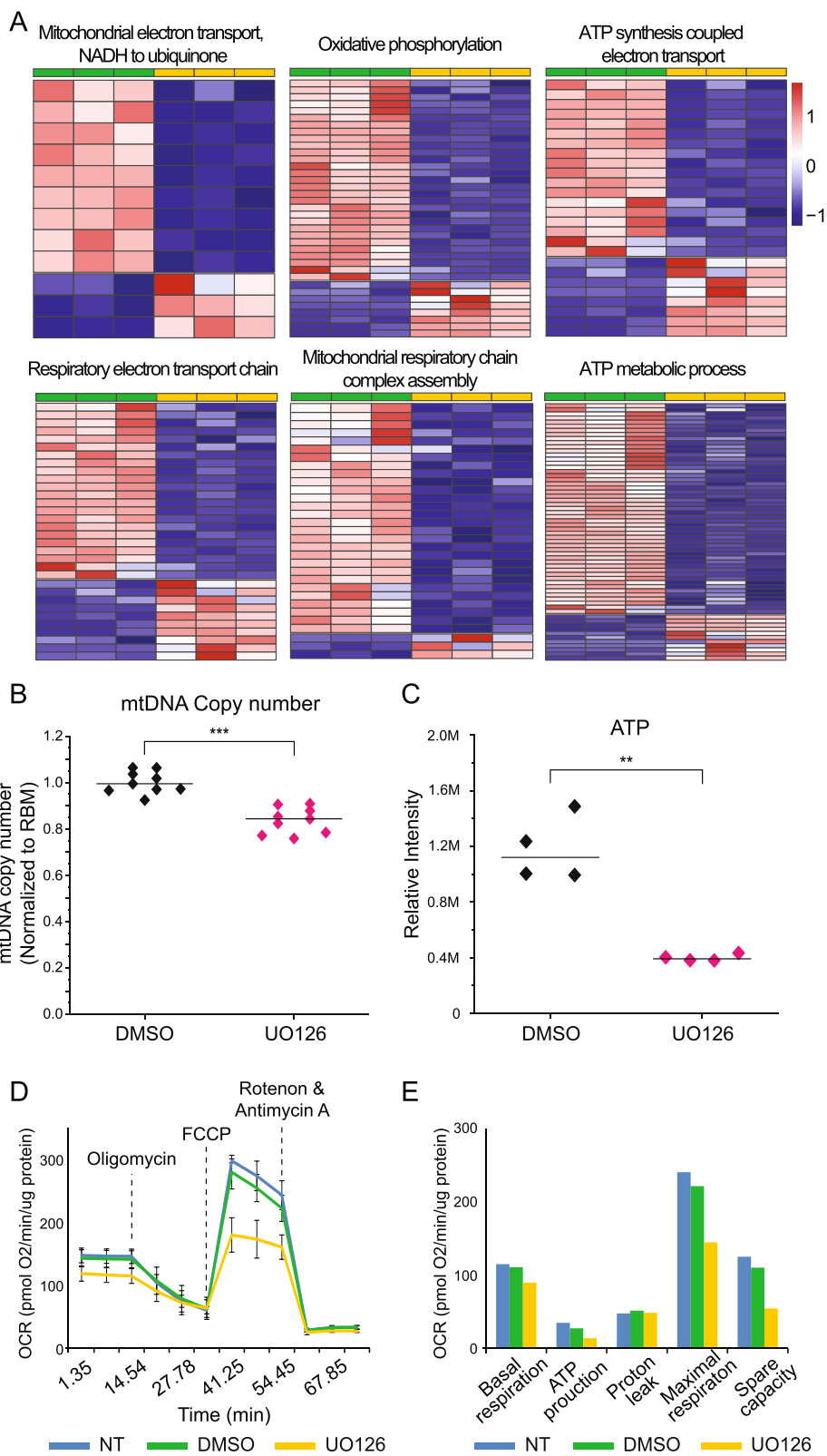


Fig. 6 (See legend on previous page.)

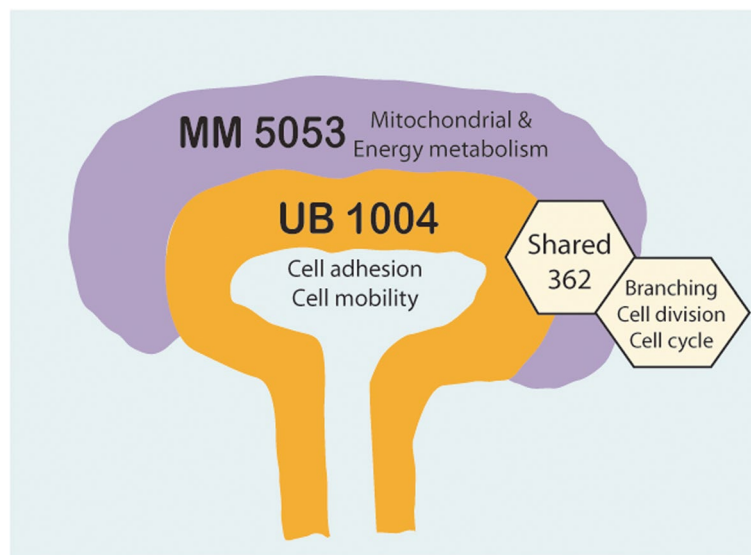


Fig. 7 Schematic summary of MAPK/ERK functions in renal progenitor populations. With the help of RNA-Seq and tissue-specific *Mek1/2* knockout, kidneys representing MAPK/ERK-deficient ureteric bud (UB) epithelium (orange) and nephron progenitor cells (purple), 1004 and 5053 differentially expressed genes were identified in MM and UB, respectively. Major changes in MM have a profound association with mitochondrial and energy metabolism. In the UB, the majority of changes correlate with cell adhesion and cell mobility functions which our further experimentation demonstrates to result in failure to maintain tip identity, resulting in the premature differentiation of the collecting duct epithelium (not shown here). Most of the changes in the 362 shared genes are related to branching, cell division, and cell cycle

Ccm2). Interestingly, MAPK/ERK-deficient MM also showed increased expression of *FoxD1* and some other Fox genes possibly suggesting lineage confusion in the absence of MAPK/ERK activation.

The interactions between ERK and chromatin have been characterized in several cell and tissue types, including both human and mouse embryonic stem cells, where ERK targets histone and other transcriptional control genes [100, 101] to regulate nucleosome assembly and chromatin availability. Similar global changes as we detected in nucleosome and chromatin assembly/organization were also revealed at least in embryonic lung and placenta development [6, 102]. Moreover, sustained MEK inhibition or its genetic loss in embryonic stem cells results in epigenetic and genomic changes, which severely deteriorate the developmental potential [103]. The interactions between MAPK/ERK and chromatin are revealed here for the embryonic kidney, where 2.5% of the DEGs in UB_{dko} (25) and 1.4% of the DEGs in MM_{dko} (69) represent histones, and the largest portion (13%) of the shared downregulated DEGs fall into the chromosome condensation and nucleosome assembly category as well. DNA replication in rapidly proliferating cells requires not only histone recycling but also efficient histone transcription, which is partially ensured by their clustered localization in the genome [104, 105]. This protects newly synthesized DNA by packaging, which

is required for the maintenance of chromatin integrity in the development and differentiation [106]. The amount of histones is inherently linked to DNA content [107–109], and decreased histone transcription in the absence of MAPK/ERK activation likely relates to delays in G1/S phase cell cycle progression, which we previously reported for both mutant tissues [39, 40]. MAPK/ERK is also known to directly regulate the transcriptional machinery and chromatin structure [100, 110, 111] providing an additional mechanism for the identified differential histone expressions in UB and MM.

Recently, overall chromatin landscapes were reported for embryonic and early postnatal nephron progenitors [112], but the regulation of open and closed chromatin structures in the developing kidney remains largely unknown. We found here that the DNA methylator *Dnmt1*, which is responsible for most of the DNA methylation in mouse cells, together with *Uhrf1*, which mediates DNMT1 recruitment to DNA, are significantly downregulated in both MAPK/ERK-deficient UB and MM. UHRF1 recruits DNMT1 to DNA during the S-phase of the cell cycle to ensure the maintenance of DNA methylation marks in replicating cells [113]. Downregulation of both *Uhrf1* and *Dnmt1* suggests defects in the maintenance of methylation status and thus cell identity in the kidney progenitor cells lacking MAPK/ERK activity, as previously reported for nephron progenitors

lacking *Dnmt1* [114]. Such a mechanism behind the failure to maintain renal progenitors in the MAPK/ERK-deficient kidneys is further supported by a significant reduction of *Dot1l*, a histone 3 lysine 79 methyltransferase, specifically in nephron progenitors, where *Dot1l* function was recently shown indispensable for their maintenance and differentiation [115].

Our RNA-Seq results in UB_{dko} showed that in the absence of MAPK/ERK, the UB tip progenitors have decreased expression of several genes which are previously shown to be tip-specific and simultaneously upregulate many of the known stalk-specific genes [30]. Furthermore, GO biological process analysis revealed 62 genes involved in the negative regulation of cell differentiation and 25 genes involved in stem cell differentiation. Most of these genes are well characterized as regulators of progenitor state and self-renewal, notably in cell types of the developing kidney are *Sema3a* [116], *Shh* [76, 117], and *Dnmt1* [114]. Together, these suggest that MAPK/ERK activity in the UB tips is required for the maintenance of tip cells and possibly for collecting duct progenitor characteristics, as in the absence of MAPK/ERK activation, they become transcriptionally more like UB stalk cells. Indeed, our protein level analysis verified the RNA-Seq-identified transcriptional changes in the UB-specific model of MAPK/ERK deficiency and revealed premature and ectopic differentiation of principal and intercalated collecting duct cells in the UB tips. Such a requirement for MAPK/ERK activation in tip cell identity is further supported by the finding that the MAPK/ERK pathway mediates GDNF's regulatory effect on collecting duct progenitors [36]. The loss of tip/progenitor identity also explains our previous observations that in the absence of MAPK/ERK activation, the UB tip cells fail to expand and generate new branches [39].

Transcriptional profiling of nephron progenitors identified a remarkable amount of DEGs related to proliferation and mitochondrial metabolism. Defects in mitochondrial function may cause apoptosis, and we observed decreased dko cell yields (38% in UB and 63% in MM) in FACS used for RNA-Seq. However, our earlier studies have demonstrated that cell death is not primarily affected in either of the genetic model kidneys [39, 40] supporting the deficits in energy metabolism. It has been reported that energy source influences the renewal-differentiation balance in nephron progenitors, which prematurely differentiate if glycolysis is prevented [118]. Our analysis showed that the overall mitochondria amount per cell in MAPK/ERK-deficient cells is reduced, which may perturb normal energy source balance in highly proliferative nephron progenitors due to diminished use of pyruvate for oxidative phosphorylation. Previously, p53, one of the well-known MAPK/ERK targets [90] also

downregulated in our MM_{dko} dataset, was shown to regulate energy metabolism in nephron progenitors [119]. Interestingly, the nephron progenitors lacking p53 are rapidly diminished, disorganized, and show defects in cellular adhesion, thus closely resembling the phenotype we have described for MAPK/ERK-deficient nephron progenitors [40]. Taken together, the MAPK/ERK pathway likely contributes to the regulation of nephron progenitor self-renewal and maintenance through its effects on ATP availability and energy metabolism, which will be further characterized in future studies.

Conclusions

With the help of the transcriptional MAPK/ERK target identification, we reveal here new mechanisms through which extracellularly induced guidance cues are mediated to two tissues of developing kidney, namely the branching ureteric bud epithelium and nephron progenitors. Our results show that MAPK/ERK activity in the tips of the UB protects epithelial cells from premature differentiation and thus allows continuous kidney growth through repeated tip bifurcation needed for new branching events [39]. Our RNA-Seq data suggests that the maintenance of collecting duct progenitor cell identity in the tips of the UB epithelium depends on the active MAPK/ERK cascade. We verified this at the protein level and show that in the absence of MAPK/ERK activity, the epithelial cells prematurely differentiate into collecting duct cell types, thus losing the capacity to branch and grow. This suggests that MAPK/ERK activity operates as a rather late gatekeeper of undifferentiated versus differentiated fate.

Our experimental data in the nephron progenitors demonstrate that MAPK/ERK activation maintains normal mitochondrial turnover and thus their metabolism that is required in these highly proliferative embryonic progenitors [120]. Based on the identified differences in the target gene signatures between ureteric bud and nephron progenitors, we suggest earlier function for MAPK/ERK activity in nephron progenitor cell fate decision hierarchy. This is supported by many other tissue-specific stem cells showing energy dependence similar to nephron progenitors, which together with the known functions of MAPK/ERK in the regulation of cell cycle progression, suggests mitochondrial energy regulation as a general mechanism through which MAPK/ERK pathway controls cellular turnover [89, 121, 122].

Methods

Mouse lines, kidney dissection, and tissue-specific cell isolation

Six2-TGC, *HoxB7*Cre-GFP, *Mek1*-floxed, and *Mek2*-null mice and their genotyping have been described previously [9, 18, 123, 124]. Mice are kept in mixed

genetic backgrounds containing C57BL6/Rcc and 129/SvEv strains. Animal husbandry and procedures were approved by the EU legislation and the Finnish Animal Care and Use Committee. For sequencing, metanephric kidneys were dissected from E12.5 *HoxB7Cre-GFP* and E13.5 *Six2-TGC* embryos. Genotypes were analyzed by PCR. Experimental samples were tissue-specifically null for all four *Mek1/2* alleles (referred to as dko, double knockout), *HoxB7Cre-GFP;Mek1^{fl/fl};Mek2^{-/-}* (UB_{dko}) and *Six2-TGC;Mek1^{fl/fl};Mek2^{-/-}* (MM_{dko}). Control samples for the MM were *Six2-TGC;Mek1^{fl/+};Mek2^{+/+}* and *Six2-TGC;Mek1^{fl/+};Mek2^{+/-}*, and controls for the UB were *HoxB7Cre-GFP;Mek1^{fl/+};Mek2^{+/-}*, *HoxB7Cre-GFP;Mek1^{+/+};Mek2^{+/-}*, and *HoxB7Cre-GFP;Mek1^{fl/+};Mek2^{+/+}*. Both kidneys from each embryo were combined, dissociated using 0.25% trypsin-EDTA with gentle pipette aspiration, and FAC-sorted based on endogenous GFP expression using a Sony SH800Z Cell Sorter.

RNA isolation for sequencing and data analysis

RNA for sequencing was isolated from FAC-sorted cells by a standard protocol for chloroform/isopropanol extraction. Isolated RNA was treated with DNase I, following the manufacturer's instructions (Thermo Fisher Scientific—04/2016, rev. B.00) with phenol/chloroform extraction. Total RNA quality and quantity were estimated by using the Bioanalyzer RNA Total Pico (Agilent Technologies, Inc.) and Nanodrop analysis. Examples of quality assurance are shown in Additional file 1: Fig. S5.

Library preparation was done using NuGen Ovation Solo. The NuGen kit with single-end reads is such that the library is first generated, after which ribosomal RNA is removed before amplification and sequencing with random primers. Sequencing with NextSeq was performed at BIDGEN DNA Sequencing and Genomics Laboratory (University of Helsinki). bcl2fastq2 Conversion Software was used to convert BCL files to FASTQ file format and demultiplex samples. Sequenced reads were trimmed for adaptor sequence and masked for low-complexity or low-quality sequence using Trimmomatic. Trimmed reads were mapped to GENCODE Mus musculus Release M23 reference genome GRCm38 using STAR aligner (2.6.0c). Counts per gene were calculated using featureCounts included as a part of the subread package [125] using the GENCODE Mus musculus Release M23 annotation file.

After receiving the matrix of raw gene counts, the data was normalized using DESeq2 R-package (v.3.6.2) [41], and the sample clustering was visually inspected by drawing PCA plots to detect possible sample outliers. The DESeq2 package uses a negative binomial generalized linear model to detect differentially expressed genes from the data. As part of the analysis, DESeq2 also performs

independent filtering where the mean of normalized counts is used as a filter statistic. This step removes genes with insufficient expression levels and in addition samples with extreme count outliers are detected by Cook's distance. Finally, multiple testing adjustment of *p*-values is done with the Benjamini-Hochberg procedure. From the *Six2-TGC* mice, three control and three dko samples were compared. From the *HoxB7Cre-GFP* mice, four control and four dko samples were compared. All control samples contained Cre and at least two *Mek* alleles. The results were filtered to include genes with a fold change greater than 2 ($|\log_2FC| \geq 1$) and false discovery rate $P_{adj} < 0.05$.

Tissue cultures and RNA isolation for qPCR

E12.5 kidneys and lungs were cultured on filters in a Trowell-type system for 24 h in the presence of 15 μ M U0126 chemical inhibitor or the same volume of DMSO vehicle control, as described previously [39]. For tissue-specific qPCR validation, UBs and MMs were manually isolated after enzymatic collagenase treatment by microdissection from E12.5 kidneys [126]. Previously reported culture mediums supplemented with 15 μ M U0126 or equal amount of DMSO were used for 3-h culture of both tissues: 50 ng/ml HGF, 5 ng/ml GDNF, 25 ng/ml FGF2 for UBs [126], and 50ng/ml FGF for MM [127]. Tissues were dissociated in TRIzol Reagent (Invitrogen) assisted by aspiration through a 25-gauge needle. RNA was isolated for whole embryonic kidneys and lungs following the same procedure as above (extraction from FAC-sorted cells). Complementary DNA was generated from total RNA (1–5 μ g per reaction) with the SuperScript IV first-strand synthesis system, following the manufacturer's instructions (Invitrogen—07/2017, rev. A.0).

The livers from three adult C57BL6 mice were sliced to 5 mm diameter and 150 μ m thickness. Three precision-cut slices per condition were cultured for 24 h with 15 μ M U0126 or equal volume DMSO. All three precision-cut slices per condition were combined in TRIzol, and RNA isolation and reverse transcription were performed in the same manner as above.

Quantitative-PCR

Gene-specific primers for qPCR were designed using NCBI Primer-BLAST. Primer sequences can be found in Additional file 11: Table S10. For qPCR, we used SensiFAST SYBR No-ROX kit (Bioline) with Bio-Rad CFX384 thermal cycler. The Bio-Rad CFX Manager software was used for gene expression analysis. Relative mRNA expression levels were calculated using the comparative Ct method, and individual expression values were normalized to the expression of eukaryotic translation initiation factor 3 subunit A (*Eif3a*) and STT3, subunit of the

oligosaccharyltransferase complex, homolog B (*S. cerevisiae*) (*Stt3b*) for kidney and lung samples and to beta-actin (*Actb*) for liver samples. The results were combined from two biological replicates (kidneys, lungs, and livers originating from two separate litters or individuals), at least two technical replicates per biological replicate, and five replicates for each gene/condition combination within each run.

Functional gene enrichment analysis

For the functional gene enrichment analysis, we applied the ToppFun application from ToppGene Suite (<https://toppgene.cchmc.org>), which provides functional enrichment analysis of candidate genes in many biological categories [128, 129]. ToppFun provides a set of advanced feature annotation tools for associating functional terms with gene lists through clustering algorithms. GO enrichment was performed to analyze the DEGs identified at the functional level, with a false discovery rate set to $p < 0.05$.

Immunofluorescent staining and imaging

Kidneys were collected at the embryonic stages indicated in the text. Samples were fixed overnight in 4% paraformaldehyde (PFA), embedded in paraffin using an automated tissue processor, cut into 5- μ m-thick sections, and allowed to dry overnight. Immunofluorescent staining of paraffin sections was performed following standard protocol with xylene-alcohol deparaffination series followed by heat-induced antigen retrieval in 20 mM Tris-HCl, 1 mM EDTA buffer at pH 8.5. After cooling to room temperature, tissue sections were blocked 1 h in 50 mM Tris-HCl, 100 mM NaCl, 0.1% Tween-20, at pH 7.5 (TNT) supplemented with 10% FBS, followed by incubation with primary antibodies at 4 °C overnight, TNT washing, and 1 h incubation with secondary antibodies. Primary antibodies were used as follows: AQP2 (1:300, Sigma), CALB1 (1:800, Santa Cruz), Na/K-ATPase (1:300, Hybridoma Bank), and V-ATPaseB1/2 (1:100, Santa Cruz). Detection was performed with Alexa Fluor-conjugated secondary antibodies (1:400; Jackson Immuno Research Laboratories). Additionally, fluorescent dye Hoechst (Invitrogen) was used at 1:1000 dilution. Epifluorescence imaging was performed with Zeiss Axio Imager.M2 outfitted with Hamamatsu Orca Flash 4.0 LT B&W camera and Zeiss Zen 2 software.

Metabolite extraction from cultured cells

The mK4 cell line originally derived from embryonic kidney mesenchyme was cultured as previously described [130]. U0126 (15 μ M) was used to mimic genetic MEK ablation in the cell line [39], and after 24-h treatment, cells were harvested with 0.25% Trypsin-EDTA, and cell

pellets were applied to metabolite extraction for ATP quantification by double phase methanol-chloroform extraction [131]. In brief, cell pellets were re-suspended with 600 μ l of methanol and chloroform (2:1 v/v ratio), and two cycles of the following steps were repeated: quick frozen with liquid nitrogen for 60s, thawing at room temperature for 2 min. After two cycles, 200 μ l of chloroform and 200 μ l of distilled water were added, and samples were centrifuged at 15,000g for 20 min at 4 °C. The upper water-soluble phase was collected and dried with a centrifugal vacuum evaporator. The protein aggregates in the middle phase were collected and re-solubilized with 6 M urea buffer for total protein concentration measurement. After speed vacuum, the dried pellets were stored at -80 °C until analysis.

ATP measurement by liquid chromatography-mass spectrometry (LC-MS)

Frozen cell metabolite extracts were dissolved in 200 μ l solvent (water:acetonitrile = 1:1 v/v ratio) and centrifuged at 15,000g for 10 min at 4 °C before injection to LC-MS. Chromatographic separation was performed on a ZIC-HILIC column (3.5 μ m, 200 Å, 100 \times 2.1 mm; Merck Millipore) using an Acquity UPLC system (Waters, MA, USA). The column temperature was 35 °C with a flow rate of 0.4 mL/min and the auto-sampler cooler temperature was set at 4 °C with an injection volume of 2 μ l. Analytes were eluted with a mobile phase composed of 10 mM ammonium acetate in water with pH 6.8 (A) and 10 mM ammonium acetate in water:acetonitrile solution (1:3) with pH 6.8 (B). Gradient conditions were as follows: 0–1 min kept B as 100%, 1–7 min declined B from 100 to 20%, 7–11 min kept B as 20%, 11.1 min set B as 100%, and kept the composition until 23 min. Mass spectrometry experiments were performed on a Q Exactive Focus Orbitrap Mass Spectrometer (Thermo Fisher Scientific) equipped with HESI sources. Data were acquired in negative mode. The measurement conditions were as follows: HESI source spray voltage of 2.5 kV, Aux gas heater temperature of 350 °C, sheath gas flow of 50, aux gas flow of 15, sweep gas flow of 2, capillary temperature of 320 °C, and S-lens RF level of 50. Scan range for the full MS experiment was 65–975 m/z with resolution as 70,000. For the PRM experiment targeting ATP measurement, the resolution was set as 35,000 and the collision energy was 20 eV. Full MS and PRM were executed simultaneously to acquire data.

Data processing and relative quantification of ATP

The target metabolite ATP was double confirmed using the MS2 spectrum pattern compared with Metlin, an online MS database, and high-resolution m/z from the

full MS experiment. Peak intensity lists of the ATP were acquired using the Xcalibur Quan Browser software (Thermo Fisher Scientific). All data were normalized by total protein concentration before comparing in groups.

Mitochondrial DNA copy number measurement

E12.5 mouse kidneys supplemented with DMSO or 15 μ M U0126 (48 h) were cultured as described above and followed by DNA isolation. The kidneys (< 5 mg) were suspended in 600 μ l TRIzol Reagent (Invitrogen) and vortexed for 30 s for complete homogenization. One sample volume (600 μ l) of 70% ethanol was added to enhance nucleic acid precipitation. The mixture was loaded onto the RNeasy MinElute spin column and centrifuged at 8000 \times g for 15 s. The flow-through containing DNA, proteins, and other contaminants was loaded onto a NucleoSpin[®] Tissue Column (MACHEREY-NAGEL). The DNA binding, washing, and drying steps were performed according to the manufacturer's protocol (MACHEREY-NAGEL—01/2017, Rev. 17) followed by elution in 50 μ l buffer BE (5 mM Tris/HCl, pH 8.5).

The set of primers (Table S10) used for mitochondrial encoded 12S ribosomal RNA (12S rRNA) and nuclear-encoded ribosomal binding protein 15 (RBM15) were used for mitochondrial DNA (mtDNA) copy number analysis. The mtDNA copy number was calculated by normalizing 12S rRNA amount against RBM15 amount.

Seahorse analysis of mitochondrial metabolism

The cellular oxygen consumption rates (OCR) of mK4 cell line were observed using a Seahorse XF96e analyzer (Seahorse Bioscience; Agilent Technologies). The XF96e sensor cartridge activation with 200 μ l of XF96 calibrant solution buffer was performed during the overnight on non-CO₂ incubator at 37 °C. Two days before the OCR measurement, 70,000 mK4 cells/well were seeded onto the XF96 cell culture microplate and cultured in the regular culture medium (DMEM) on CO₂ incubator at 37 °C. One day after, 15 μ M of U0126 and DMSO were added, and cells were incubated for 24 h on CO₂ incubator at 37 °C. One hour prior to the OCR measurement, the medium was changed to serum-free and bicarbonate-free DMEM medium supplemented with 10 mM Glucose, 5 mM pyruvate, and 5 mM glutamine, pH 7.4, and incubated for 1 h in a non-CO₂ incubator at 37 °C. The Seahorse analyzer sequentially injected 1 μ M of oligomycin (ATP synthase inhibitor), 1 μ M of FCCP (protonophore uncoupler), and 1 μ M of Rotenone and Antimycin A (ETC inhibitors) and measured OCR before and after injection at indicated time points. The observed OCR was normalized against total protein amount (micrograms).

To determine the mitochondrial function, basal respiration, ATP production, proton leak, maximal respiration, and spare respiration capacity were calculated according to the manufacturer's instructions. In detail, non-mitochondrial respiration rate; minimum rate measurement after rotenone/antimycin A injection, basal respiration; (last rate measurement before first injection) – (non-mitochondrial respiration rate), maximal respiration; (maximum rate measurement after FCCP injection) – (non-mitochondrial respiration), proton leak; (minimum rate measurement after oligomycin injection) – (non-mitochondrial respiration), ATP production; (last rate measurement before oligomycin injection) – (minimum rate measurement after oligomycin injection), spare respiration capacity; (maximal respiration) – (basal respiration).

Abbreviations

ATP: Adenosine triphosphate; BCL: Binary base call; DEG: Differentially expressed gene; DMSO: Dimethyl sulfoxide; dko: Double-knockout; FACS: Fluorescence-activated cell sorting; FBS: Fetal bovine serum; FGF: Fibroblast growth factor; FRET: Förster (or fluorescence) resonance energy transfer; GFP: Green fluorescent protein; GDNF: Glial cell line-derived neurotrophic factor; GO: Gene Ontology; LC/MS: Liquid chromatography–mass spectrometry; MAPK/ERK: Mitogen-activated protein kinase/extracellular signal-regulated kinase; MM: Metanephric mesenchyme; MM_{dko}: MAPK-deficient metanephric mesenchyme; mtDNA: Mitochondrial DNA; qPCR: Quantitative PCR; P_{adj} : P -value adjusted; PCA: Principal component analysis; PCR: Polymerase chain reaction; PFA: Paraformaldehyde; RNA-seq: RNA sequencing; RTK: Receptor tyrosine kinase; UB: Ureteric bud; UB_{dko}: MAPK-deficient ureteric bud; U0126: Chemical MEK inhibitor; 3R: Refine, reduce, replace.

Supplementary Information

The online version contains supplementary material available at <https://doi.org/10.1186/s12915-022-01309-z>.

Additional file 1: Fig. S1. Principal component analysis (PCA) for RNA-Seq data. **Fig. S2.** Functional gene enrichment analysis of UB and MM datasets. **Fig. S3.** Quantitative PCR analysis of MAPK/ERK targets in embryonic kidney, MM and UB tissues. **Fig. S4.** Transcription factor target-enrichment in MAPK/ERK-deficient UB. **Fig. S5.** Examples of RNA quality assurance studies performed prior proceeding to sequencing of actual samples.

Additional file 2: Table S1. The differentially expressed genes in UBdko dataset.

Additional file 3: Table S2. The differentially expressed genes in MMdko dataset.

Additional file 4: Table S3. Gene ontology analysis of UBdko and MMdko datasets.

Additional file 5: Table S4. Genes differentially expressed in both UB and MM datasets.

Additional file 6: Table S5. Gene ontology analysis of shared differentially expressed genes.

Additional file 7: Table S6. Identified histone-related genes differentially expressed in UB and MM datasets.

Additional file 8: Table S7. Analysis of MAPK/ERK target genes in extra-renal tissues. The gene expression changes identified in embryonic kidney were also quantified by qPCR in E12.5 mouse lungs and adult liver slices cultured for 24h in the presence of MEK inhibitor U0126. The analyzed genes are listed in "Gene" column followed by Yes/No to indicate whether

the expression pattern observed in MAPK/ERK-deficient embryonic kidney was recapitulated in the extra-renal tissue. "Regulation" column shows whether the given gene expression was up- or down-regulated by MEK inhibition and indicates the potential statistical significance (*= $p < 0.05$; **= $p < 0.01$; ***= $p < 0.001$).

Additional file 9: Table S9. Gene list for heatmaps in Fig. 6.

Additional file 10: Table S9. Raw data values for measurements of ATP, protein amount and calculations of normalized ATP intensities.

Additional file 11: Table S10. qRT-PCR primer sequences.

Acknowledgements

We thank Dr. Outi Monni (Biomedicum Functional Genomics Unit, Faculty of Medicine, University of Helsinki, Finland) for enabling the bioinformatic analysis of RNA-Seq data. This work was carried out with the help from the following institutional core facilities that are part of the Biocenter Finland Infrastructures: Biomedicum Imaging Unit, Biomedicum Flow Cytometry, DNA Sequencing and Genomics, GM Unit and Laboratory Animal Centre, and Helsinki Life Science.

Authors' contributions

All authors read and approved the final manuscript. KK and HNK participated in the experimental planning, conducted the most experiments, and analyzed the RNA-Seq results with JV and IF. MA and IB conducted and provided the adult liver samples. TQ and HT participated in the qPCR design. KK and VI implemented the qPCR. JK and AIH collected and processed the in vivo kidney tissues for RNA-Seq. XJ and SP performed the LC-MS-based ATP measure. SK designed the study, analyzed the results, and wrote the paper together with KK and HNK.

Funding

This work was supported by funds from the Academy of Finland 309997 (SK), Jane and Aatos Erkkö Foundation (SK), the Finnish Cultural Foundation (SK; HNK), the Maud Kuistila Foundation (SK; KK), and the Orion Research Foundation (KK).

Availability of data and materials

The data supporting the findings of this study are available within the article and its supplementary materials that includes original data of ATP measurements. Specifically, RNA sequencing (RNA-seq) dataset that supports the findings of this study is available in the Gene Expression Omnibus repository, accession number GSE174229 (<https://www.ncbi.nlm.nih.gov/geo/query/acc.cgi?acc=GSE174229>) [132].

Declarations

Ethics approval and consent to participate

Mice used in these studies were maintained in a pathogen-specific free facility under the care and supervision of University of Helsinki's Institutional Animal Care and Use Committee.

Consent for publication

Not applicable.

Competing interests

The authors declare that they have no competing interests.

Author details

¹Helsinki Institute of Life Science, University of Helsinki, Helsinki, Finland. ²Stem Cells and Metabolism Research Program, Faculty of Medicine, University of Helsinki, Helsinki, Finland. ³Present address: Molecular and Integrative Biosciences Research Programme, Faculty of Biological and Environmental Sciences, University of Helsinki, Helsinki, Finland. ⁴Department of Biochemical Sciences, Faculty of Pharmacy in Hradec Králové, Charles University, Hradec Králové, Czech Republic. ⁵Natural Product Research Institute, College of Pharmacy, Seoul National University, 1 Gwanak-ro, Gwanak-gu, Seoul 08826, Korea. ⁶Present address: Department of Medical Biochemistry and Biophysics, Division of Molecular Neurobiology, Karolinska Institutet, SE-17177 Solna,

Sweden. ⁷Biomedicum Functional Genomics Unit, Helsinki Institute of Life Science and Applied Tumors Genomics Research Program, Faculty of Medicine, University of Helsinki, Helsinki, Finland. ⁸Neuroscience Center, Helsinki Institute of Life Science, University of Helsinki, Helsinki, Finland. ⁹Department of Medical and Clinical Genetics, University of Helsinki, Helsinki, Finland. ¹⁰GM-unit, Laboratory Animal Center, Helsinki Institute of Life Science, University of Helsinki, Helsinki, Finland.

Received: 28 April 2021 Accepted: 25 April 2022

Published online: 13 May 2022

References

- Zhang W, Liu HT. MAPK signal pathways in the regulation of cell proliferation in mammalian cells. *Cell Res.* 2002;12(1):9–18.
- McKay MM, Morrison DK. Integrating signals from RTKs to ERK/MAPK. *Oncogene.* 2007;26(22):3113–21.
- Roskoski R Jr. ERK1/2 MAP kinases: structure, function, and regulation. *Pharmacol Res.* 2012;66(2):105–43.
- Miller AD, Curran T, Verma IM. c-fos protein can induce cellular transformation: a novel mechanism of activation of a cellular oncogene. *Cell.* 1984;36(1):51–60.
- Guzowski JF, McNaughton BL, Barnes CA, Worley PF. Environment-specific expression of the immediate-early gene *Arc* in hippocampal neuronal ensembles. *Nat Neurosci.* 1999;2(12):1120–4.
- Boucherat O, Nadeau V, Berube-Simard FA, Charron J, Jeannotte L. Crucial requirement of ERK/MAPK signaling in respiratory tract development. *Development.* 2015;142(21):3801.
- Parada C, Han D, Grimaldi A, Sarrion P, Park SS, Pelikan R, et al. Disruption of the ERK/MAPK pathway in neural crest cells as a potential cause of Pierre Robin sequence. *Development.* 2015;142(21):3734–45.
- Dumesic PA, Scholl FA, Barragan DI, Khavari PA. Erk1/2 MAP kinases are required for epidermal G2/M progression. *J Cell Biol.* 2009;185(3):409–22.
- Scholl FA, Dumesic PA, Barragan DI, Harada K, Bissonauth V, Charron J, et al. Mek1/2 MAPK kinases are essential for mammalian development, homeostasis, and Raf-induced hyperplasia. *Dev Cell.* 2007;12(4):615–29.
- Kurtzeborn K, Kwon HN, Kuure S. MAPK/ERK signaling in regulation of renal differentiation. *Int J Mol Sci.* 2019;20(7):1779.
- Saxen L. *Organogenesis of the kidney.* Cambridge: Cambridge University Press; 1987.
- Mao Y, Francis-West P, Irvine KD. Fat4/Dchs1 signaling between stromal and cap mesenchyme cells influences nephrogenesis and ureteric bud branching. *Development.* 2015;142(15):2574–85.
- Davidson AJ, Lewis P, Przepiorski A, Sander V. Turning mesoderm into kidney. *Semin Cell Dev Biol.* 2019;91:86–93.
- Zhang H, Bagherie-Lachidan M, Badouel C, Enderle L, Peidis P, Bremner R, et al. FAT4 fine-tunes kidney development by regulating RET signaling. *Dev Cell.* 2019;48(6):780–792 e784.
- Kurtzeborn K, Cebrian C, Kuure S. Regulation of renal differentiation by trophic factors. *Front Physiol.* 2018;9:1588.
- Costantini F, Kopan R. Patterning a complex organ: branching morphogenesis and nephron segmentation in kidney development. *Dev Cell.* 2010;18(5):698–712.
- Kuure S, Sariola H. Mouse models of congenital kidney anomalies. *Adv Exp Med Biol.* 2020;1236:109–36.
- Kobayashi A, Valerius MT, Mugford JW, Carroll TJ, Self M, Oliver G, et al. Six2 defines and regulates a multipotent self-renewing nephron progenitor population throughout mammalian kidney development. *Cell Stem Cell.* 2008;3(2):169–81.
- Self M, Lagutin OV, Bowling B, Hendrix J, Cai Y, Dressler GR, et al. Six2 is required for suppression of nephrogenesis and progenitor renewal in the developing kidney. *EMBO J.* 2006;25(21):5214–28.
- Li H, Hohenstein P, Kuure S. Embryonic kidney development, stem cells and the origin of Wilms tumor. *Genes (Basel).* 2021;12(2):318.
- O'Brien LL. Nephron progenitor cell commitment: striking the right balance. *Semin Cell Dev Biol.* 2018;91:94–103.
- Rumballe BA, Georgas KM, Combes AN, Ju AL, Gilbert T, Little MH. Nephron formation adopts a novel spatial topology at cessation of nephrogenesis. *Dev Biol.* 2011;360(1):110–22.

23. Short KM, Combes AN, Lefevre J, Ju AL, Georgas KM, Lamberton T, et al. Global quantification of tissue dynamics in the developing mouse kidney. *Dev Cell*. 2014;29(2):188–202.
24. Park JS, Ma W, O'Brien LL, Chung E, Guo JJ, Cheng JG, et al. Six2 and Wnt regulate self-renewal and commitment of nephron progenitors through shared gene regulatory networks. *Dev Cell*. 2012;23(3):637–51.
25. Lindstrom NO, Carragher NO, Hohenstein P. The PI3K pathway balances self-renewal and differentiation of nephron progenitor cells through beta-catenin signaling. *Stem Cell Reports*. 2015;4(4):551–60.
26. Lawlor KT, Zappia L, Lefevre J, Park JS, Hamilton NA, Oshlack A, et al. Nephron progenitor commitment is a stochastic process influenced by cell migration. *Elife*. 2019;8:e41156.
27. Watanabe T, Costantini F. Real-time analysis of ureteric bud branching morphogenesis in vitro. *Dev Biol*. 2004;271(1):98–108.
28. Schmidt-Ott KM, Yang J, Chen X, Wang H, Paragas N, Mori K, et al. Novel regulators of kidney development from the tips of the ureteric bud. *J Am Soc Nephrol*. 2005;16(7):1993–2002.
29. Bohnenpoll T, Kispert A. Ureter growth and differentiation. *Semin Cell Dev Biol*. 2014;36:21–30.
30. Rutledge EA, Benazet JD, McMahon AP. Cellular heterogeneity in the ureteric progenitor niche and distinct profiles of branching morphogenesis in organ development. *Development*. 2017;144(17):3177–88.
31. Lefevre JG, Short KM, Lamberton TO, Michos O, Graf D, Smyth IM, et al. Branching morphogenesis in the developing kidney is governed by rules that pattern the ureteric tree. *Development*. 2017;144(23):4377–85.
32. Short KM, Smyth IM. Branching morphogenesis as a driver of renal development. *Anat Rec (Hoboken)*. 2020;303(10):2578–87.
33. Shakya R, Watanabe T, Costantini F. The role of GDNF/Ret signaling in ureteric bud cell fate and branching morphogenesis. *Dev Cell*. 2005;8(1):65–74.
34. Chi X, Michos O, Shakya R, Riccio P, Enomoto H, Licht JD, et al. Ret-dependent cell rearrangements in the Wolffian duct epithelium initiate ureteric bud morphogenesis. *Dev Cell*. 2009;17(2):199–209.
35. Riccio P, Cebrian C, Zong H, Hippenmeyer S, Costantini F. Ret and Etv4 promote directed movements of progenitor cells during renal branching morphogenesis. *PLoS Biol*. 2016;14(2):e1002382.
36. Li H, Jakobson M, Ola R, Gui Y, Kumar A, Sipila P, et al. Development of the urogenital system is regulated via the 3'UTR of GDNF. *Sci Rep*. 2019;9(1):5302.
37. Hida M, Omori S, Awazu M. ERK and p38 MAP kinase are required for rat renal development. *Kidney Int*. 2002;61(4):1252–62.
38. Fisher CE, Michael L, Barnett MW, Davies JA. Erk MAP kinase regulates branching morphogenesis in the developing mouse kidney. *Development*. 2001;128(21):4329–38.
39. Ihermann-Hella A, Lume M, Miinalainen IJ, Pirttiniemi A, Gui Y, Peranen J, et al. Mitogen-activated protein kinase (MAPK) pathway regulates branching by remodeling epithelial cell adhesion. *PLoS Genet*. 2014;10(3):e1004193.
40. Ihermann-Hella A, Hirashima T, Kupari J, Kurtzeborn K, Li H, Kwon HN, et al. Dynamic MAPK/ERK activity sustains nephron progenitors through niche regulation and primes precursors for differentiation. *Stem Cell Reports*. 2018;11(4):912–28.
41. Love MI, Huber W, Anders S. Moderated estimation of fold change and dispersion for RNA-seq data with DESeq2. *Genome Biol*. 2014;15(12):550.
42. Sanchez-Ferras O, Pacis A, Sotiropoulou M, Zhang Y, Wang YC, Bourgey M, et al. A coordinated progression of progenitor cell states initiates urinary tract development. *Nat Commun*. 2021;12(1):2627.
43. Lindstrom NO, De Sena BG, Tran T, Ransick A, Suh G, Guo J, et al. Progressive recruitment of mesenchymal progenitors reveals a time-dependent process of cell fate acquisition in mouse and human nephrogenesis. *Dev Cell*. 2018;45(5):651–660 e654.
44. Menon R, Otto EA, Kokoruda A, Zhou J, Zhang Z, Yoon E, et al. Single-cell analysis of progenitor cell dynamics and lineage specification in the human fetal kidney. *Development*. 2018;145(16):dev164038.
45. Brunskill EW, Park JS, Chung E, Chen F, Magella B, Potter SS. Single cell dissection of early kidney development: multilineage priming. *Development*. 2014;141(15):3093–101.
46. Hanafusa H, Torii S, Yasunaga T, Nishida E. Sprout1 and Sprout2 provide a control mechanism for the Ras/MAPK signalling pathway. *Nat Cell Biol*. 2002;4(11):850–8.
47. Hernandez VJ, Weng J, Ly P, Pompey S, Dong H, Mishra L, et al. Cavin-3 dictates the balance between ERK and Akt signaling. *Elife*. 2013;2:e00905.
48. Mah SP, Saueressig H, Goulding M, Kintner C, Dressler GR. Kidney development in cadherin-6 mutants: delayed mesenchyme-to-epithelial conversion and loss of nephrons. *Dev Biol*. 2000;223(1):38–53.
49. Airik R, Trowe MO, Foik A, Farin HF, Petry M, Schuster-Gossler K, et al. Hydronephrosis due to loss of Sox9-regulated smooth muscle cell differentiation of the ureteric mesenchyme. *Hum Mol Genet*. 2010;19(24):4918–29.
50. Reginensi A, Clarkson M, Neirijnck Y, Lu B, Ohshima T, Groves AK, et al. SOX9 controls epithelial branching by activating RET effector genes during kidney development. *Hum Mol Genet*. 2011;20(6):1143–53.
51. Kumar S, Liu J, Pang P, Krautzberger AM, Reginensi A, Akiyama H, et al. Sox9 activation highlights a cellular pathway of renal repair in the acutely injured mammalian kidney. *Cell Rep*. 2015;12(8):1325–38.
52. Basson MA, Akbulut S, Watson-Johnson J, Simon R, Carroll TJ, Shakya R, et al. Sprout1 is a critical regulator of GDNF/RET-mediated kidney induction. *Dev Cell*. 2005;8(2):229–39.
53. Roskoski R Jr. Targeting ERK1/2 protein-serine/threonine kinases in human cancers. *Pharmacol Res*. 2019;142:151–68.
54. Lu BC, Cebrian C, Chi X, Kuure S, Kuo R, Bates CM, et al. Etv4 and Etv5 are required downstream of GDNF and Ret for kidney branching morphogenesis. *Nat Genet*. 2009;41(12):1295–302.
55. Kuure S, Chi X, Lu B, Costantini F. The transcription factors Etv4 and Etv5 mediate formation of the ureteric bud tip domain during kidney development. *Development*. 2010;137(12):1975–9.
56. Jeffrey KL, Camps M, Rommel C, Mackay CR. Targeting dual-specificity phosphatases: manipulating MAP kinase signalling and immune responses. *Nat Rev Drug Discov*. 2007;6(5):391–403.
57. Davies JA. The Kidney Development Database. *Dev Genet*. 1999;24(3–4):194–8.
58. Majumdar A, Vainio S, Kispert A, McMahon J, McMahon AP. Wnt11 and Ret/Gdnf pathways cooperate in regulating ureteric branching during metanephric kidney development. *Development*. 2003;130(14):3175–85.
59. O'Brien LL, Combes AN, Short KM, Lindstrom NO, Whitney PH, Cullen-McEwen LA, et al. Wnt11 directs nephron progenitor polarity and motile behavior ultimately determining nephron endowment. *Elife*. 2018;7:e40392.
60. Rutledge EA, Parvez RK, Short KM, Smyth IM, McMahon AP. Morphogenesis of the kidney and lung requires branch-tip directed activity of the Adamts18 metalloprotease. *Dev Biol*. 2019;454(2):156–69.
61. Nishita M, Qiao S, Miyamoto M, Okinaka Y, Yamada M, Hashimoto R, et al. Role of Wnt5a-Ror2 signaling in morphogenesis of the metanephric mesenchyme during ureteric budding. *Mol Cell Biol*. 2014;34(16):3096–105.
62. Schuchardt A, D'Agati V, Larsson-Blomberg L, Costantini F, Pachnis V. Defects in the kidney and enteric nervous system of mice lacking the tyrosine kinase receptor Ret. *Nature*. 1994;367(6461):380–3.
63. Costantini F. Genetic controls and cellular behaviors in branching morphogenesis of the renal collecting system. *Wiley Interdiscip Rev Dev Biol*. 2012;1(5):693–713.
64. Zhang S, Lin Y, Itaranta P, Yagi A, Vainio S. Expression of Sprout genes 1, 2 and 4 during mouse organogenesis. *Mech Dev*. 2001;109(2):367–70.
65. Rutledge EA, McMahon AP. Mutational analysis of genes with ureteric progenitor cell-specific expression in branching morphogenesis of the mouse kidney. *Dev Dyn*. 2020;249(6):765–74.
66. Stanton BR, Perkins AS, Tessarollo L, Sassoon DA, Parada LF. Loss of N-myc function results in embryonic lethality and failure of the epithelial component of the embryo to develop. *Genes Dev*. 1992;6(12):2235–47.
67. Hohenstein P, Pritchard-Jones K, Charlton J. The yin and yang of kidney development and Wilms' tumors. *Genes Dev*. 2015;29(5):467–82.
68. Pan X, Karner CM, Carroll TJ. Myc cooperates with beta-catenin to drive gene expression in nephron progenitor cells. *Development*. 2017;144(22):4173–82.

69. Cacalano G, Farinas I, Wang LC, Hagler K, Forgie A, Moore M, et al. GFR α 1 is an essential receptor component for GDNF in the developing nervous system and kidney. *Neuron*. 1998;21(1):53–62.
70. Enomoto H, Araki T, Jackman A, Heuckeroth RO, Snider WD, Johnson EMJ, et al. GFR α 1-deficient mice have deficits in the enteric nervous system and kidneys. *Neuron*. 1998;21(2):317–24.
71. Jadeja S, Smyth I, Pitera JE, Taylor MS, van Haelst M, Bentley E, et al. Identification of a new gene mutated in Fraser syndrome and mouse myelencephalic blebs. *Nat Genet*. 2005;37(5):520–5.
72. Kiyozumi D, Takeichi M, Nakano I, Sato Y, Fukuda T, Sekiguchi K. Basement membrane assembly of the integrin α 8 β 1 ligand nephronectin requires Fraser syndrome-associated proteins. *J Cell Biol*. 2012;197(5):677–89.
73. Magella B, Adam M, Potter AS, Venkatasubramanian M, Chetal K, Hay SB, et al. Cross-platform single cell analysis of kidney development shows stromal cells express Gdnf. *Dev Biol*. 2018;434(1):36–47.
74. Williere Y, Borschewski A, Patzak A, Nikitina T, Dittmayer C, Daigeler AL, et al. Caveolin 1 promotes renal water and salt reabsorption. *Sci Rep*. 2018;8(1):545.
75. He JZ, Yang BX. Aquaporins in renal diseases. *Int J Mol Sci*. 2019;20(2):366.
76. Gill PS, Rosenblum ND. Control of murine kidney development by sonic hedgehog and its Gli effectors. *Cell Cycle*. 2006;5(13):1426–30.
77. Sandilands A, Smith FJ, Lunny DP, Campbell LE, Davidson KM, MacCallum SF, et al. Generation and characterisation of keratin 7 (K7) knockout mice. *PLoS One*. 2013;8(5):e64404.
78. Chen L, Lee JW, Chou CL, Nair AV, Battistone MA, Paunescu TG, et al. Transcriptomes of major renal collecting duct cell types in mouse identified by single-cell RNA-seq. *Proc Natl Acad Sci U S A*. 2017;114(46):E9989–98.
79. Pinto JP, Kalathur RK, Oliveira DV, Barata T, Machado RS, Machado S, et al. StemChecker: a web-based tool to discover and explore stemness signatures in gene sets. *Nucleic Acids Res*. 2015;43(W1):W72–7.
80. Takahashi K, Yamanaka S. Induction of pluripotent stem cells from mouse embryonic and adult fibroblast cultures by defined factors. *Cell*. 2006;126(4):663–76.
81. Bouchard C, Dittrich O, Kiermaier A, Dohmann K, Menkel A, Eilers M, et al. Regulation of cyclin D2 gene expression by the Myc/Max/Mad network: Myc-dependent TRRAP recruitment and histone acetylation at the cyclin D2 promoter. *Gene Dev*. 2001;15(16):2042–7.
82. Dyson N. The regulation of E2F by pRB-family proteins. *Gene Dev*. 1998;12(15):2245–62.
83. Margueron R, Reinberg D. The Polycomb complex PRC2 and its mark in life. *Nature*. 2011;469(7330):343–9.
84. Boyer LA, Plath K, Zeitlinger J, Brambrink T, Medeiros LA, Lee TI, et al. Polycomb complexes repress developmental regulators in murine embryonic stem cells. *Nature*. 2006;441(7091):349–53.
85. Roy A, Al-Bataineh MM, Pastor-Soler NM. Collecting duct intercalated cell function and regulation. *Clin J Am Soc Nephrol*. 2015;10(2):305–24.
86. Guo Q, Wang Y, Tripathi P, Manda KR, Mukherjee M, Chaklader M, et al. Adam10 mediates the choice between principal cells and intercalated cells in the kidney. *J Am Soc Nephrol*. 2015;26(1):149–59.
87. Willecke R, Heuberger J, Grossmann K, Michos O, Schmidt-Ott K, Walentin K, et al. The tyrosine phosphatase Shp2 acts downstream of GDNF/Ret in branching morphogenesis of the developing mouse kidney. *Dev Biol*. 2011;360(2):310–7.
88. Wilson MZ, Ravindran PT, Lim WA, Toettcher JE. Tracing information flow from Erk to target gene induction reveals mechanisms of dynamic and combinatorial control. *Mol Cell*. 2017;67(5):757–769 e755.
89. Johnson HE, Toettcher JE. Signaling dynamics control cell fate in the early Drosophila embryo. *Dev Cell*. 2019;48(3):361–370 e363.
90. De S, Campbell C, Venkitaraman AR, Esposito A. Pulsatile MAPK signaling modulates p53 activity to control cell fate decisions at the G2 checkpoint for DNA damage. *Cell Rep*. 2020;30(7):2083–2093 e2085.
91. Kamioka Y, Sumiyama K, Mizuno R, Sakai Y, Hirata E, Kiyokawa E, et al. Live imaging of protein kinase activities in transgenic mice expressing FRET biosensors. *Cell Struct Funct*. 2012;37(1):65–73.
92. Stuart RO, Bush KT, Nigam SK. Changes in global gene expression patterns during development and maturation of the rat kidney. *Proc Natl Acad Sci U S A*. 2001;98(10):5649–54.
93. Mortazavi A, Williams BA, McCue K, Schaeffer L, Wold B. Mapping and quantifying mammalian transcriptomes by RNA-Seq. *Nat Methods*. 2008;5(7):621–8.
94. Brunskill EW, Potter SS. RNA-Seq defines novel genes, RNA processing patterns and enhancer maps for the early stages of nephrogenesis: Hox supergenes. *Dev Biol*. 2012;368(1):4–17.
95. Bishop JM, Capobianco AJ, Doyle HJ, Finney RE, McMahon M, Robbins SM, et al. Proto-oncogenes and plasticity in cell signaling. *Cold Spring Harb Symp Quant Biol*. 1994;59:165–71.
96. Marshall CJ. Specificity of receptor tyrosine kinase signaling: transient versus sustained extracellular signal-regulated kinase activation. *Cell*. 1995;80(2):179–85.
97. Costantini F. GDNF/Ret signaling and renal branching morphogenesis: From mesenchymal signals to epithelial cell behaviors. *Organogenesis*. 2010;6(4):252–62.
98. Walker KA, Sims-Lucas S, Bates CM. Fibroblast growth factor receptor signaling in kidney and lower urinary tract development. *Pediatr Nephrol*. 2016;31(6):885–95.
99. Lin EE, Sequeira-Lopez MLS, Gomez RA. RBP-J in FOXD1 $^{+}$ renal stromal progenitors is crucial for the proper development and assembly of the kidney vasculature and glomerular mesangial cells. *Am J Physiol-Renal*. 2014;306(2):F249–58.
100. Tee WW, Shen SS, Oksuz O, Narendra V, Reinberg D. Erk1/2 activity promotes chromatin features and RNAPII phosphorylation at developmental promoters in mouse ESCs. *Cell*. 2014;156(4):678–90.
101. Goke J, Chan YS, Yan J, Vingron M, Ng HH. Genome-wide kinase-chromatin interactions reveal the regulatory network of ERK signaling in human embryonic stem cells. *Mol Cell*. 2013;50(6):844–55.
102. Nadeau V, Charron J. Essential role of the ERK/MAPK pathway in blood-placental barrier formation. *Development*. 2014;141(14):2825–37.
103. Choi J, Huebner AJ, Clement K, Walsh RM, Savol A, Lin K, et al. Prolonged Mek1/2 suppression impairs the developmental potential of embryonic stem cells. *Nature*. 2017;548(7666):219–23.
104. Corpet A, Almouzni G. Making copies of chromatin: the challenge of nucleosomal organization and epigenetic information. *Trends Cell Biol*. 2009;19(1):29–41.
105. Almouzni G, Cedar H. Maintenance of epigenetic information. *Cold Spring Harb Perspect Biol*. 2016;8(5):a019372.
106. Mendiatta S, Gatto A, Almouzni G. Histone supply: multitiered regulation ensures chromatin dynamics throughout the cell cycle. *J Cell Biol*. 2019;218(1):39–54.
107. Armstrong C, Spencer SL. Replication-dependent histone biosynthesis is coupled to cell-cycle commitment. *Proc Natl Acad Sci U S A*. 2021;118(31):e2100178118.
108. Claude KL, Bureik D, Chatzitheodoridou D, Adarska P, Singh A, Schmoller KM. Transcription coordinates histone amounts and genome content. *Nat Commun*. 2021;12(1):4202.
109. MacAlpine DM, Almouzni G. Chromatin and DNA replication. *Cold Spring Harb Perspect Biol*. 2013;5(8):a010207.
110. Whitmarsh AJ. Regulation of gene transcription by mitogen-activated protein kinase signaling pathways. *Biochim Biophys Acta*. 2007;1773(8):1285–98.
111. Yue J, Lai F, Beckedorff F, Zhang A, Pastor C, Shiekhhattar R. Integrator orchestrates RAS/ERK1/2 signaling transcriptional programs. *Genes Dev*. 2017;31(17):1809–20.
112. Hilliard S, Song R, Liu H, Chen CH, Li Y, Baddoo M, et al. Defining the dynamic chromatin landscape of mouse nephron progenitors. *Biol Open*. 2019;8(5):bio042754.
113. Nishiyama A, Mulholland CB, Bultmann S, Kori S, Endo A, Saeki Y, et al. Two distinct modes of DNMT1 recruitment ensure stable maintenance DNA methylation. *Nat Commun*. 2020;11(1):1222.
114. Wanner N, Vornweg J, Combes A, Wilson S, Plappert J, Rafflenbeul G, et al. DNA methyltransferase 1 controls nephron progenitor cell renewal and differentiation. *J Am Soc Nephrol*. 2019;30(1):63–78.
115. Wang F, Ngo J, Li Y, Liu H, Chen CH, Saifudeen Z, et al. Targeted disruption of the histone lysine 79 methyltransferase Dot1L in nephron progenitors causes congenital renal dysplasia. *Epigenetics*. 2020;16:1–16.
116. Reidy KJ, Villegas G, Teichman J, Veron D, Shen W, Jimenez J, et al. Semaphorin3a regulates endothelial cell number and podocyte differentiation during glomerular development. *Development*. 2009;136(23):3979–89.

117. Yu J, Carroll TJ, McMahon AP. Sonic hedgehog regulates proliferation and differentiation of mesenchymal cells in the mouse metanephric kidney. *Development*. 2002;129(22):5301–12.
118. Liu J, Edgington-Giordano F, Dugas C, Abrams A, Katakam P, Satou R, et al. Regulation of nephron progenitor cell self-renewal by intermediary metabolism. *J Am Soc Nephrol*. 2017;28(11):3323–35.
119. Li Y, Liu J, Li W, Brown A, Baddoo M, Li M, et al. p53 enables metabolic fitness and self-renewal of nephron progenitor cells. *Development*. 2015;142(7):1228–41.
120. Moussaieff A, Rouleau M, Kitsberg D, Cohen M, Levy G, Barasch D, et al. Glycolysis-mediated changes in acetyl-CoA and histone acetylation control the early differentiation of embryonic stem cells. *Cell Metab*. 2015;21(3):392–402.
121. Shyh-Chang N, Ng HH. The metabolic programming of stem cells. *Genes Dev*. 2017;31(4):336–46.
122. Mizukami Y, Iwamatsu A, Aki T, Kimura M, Nakamura K, Nao T, et al. ERK1/2 regulates intracellular ATP levels through alpha-enolase expression in cardiomyocytes exposed to ischemic hypoxia and reoxygenation. *J Biol Chem*. 2004;279(48):50120–31.
123. Zhao H, Kegg H, Grady S, Truong HT, Robinson ML, Baum M, et al. Role of fibroblast growth factor receptors 1 and 2 in the ureteric bud. *Dev Biol*. 2004;276(2):403–15.
124. Belanger LF, Roy S, Tremblay M, Brott B, Steff AM, Mourad W, et al. Mek2 is dispensable for mouse growth and development. *Mol Cell Biol*. 2003;23(14):4778–87.
125. Liao Y, Smyth GK, Shi W. featureCounts: an efficient general purpose program for assigning sequence reads to genomic features. *Bioinformatics*. 2014;30(7):923–30.
126. Kuure S. Analysis of migration in primary ureteric bud epithelial cells. *Methods Mol Biol*. 2012;886:147–55.
127. Barasch J, Yang J, Ware CB, Taga T, Yoshida K, Erdjument-Bromage H, et al. Mesenchymal to epithelial conversion in rat metanephros is induced by LIF. *Cell*. 1999;99(4):377–86.
128. Chen J, Bardes EE, Aronow BJ, Jegga AG. ToppGene Suite for gene list enrichment analysis and candidate gene prioritization. *Nucleic Acids Res*. 2009;37(Web Server issue):W305–11.
129. Zhao Z, Guo AY, van den Oord EJ, Aliev F, Jia P, Edenberg HJ, et al. Multi-species data integration and gene ranking enrich significant results in an alcoholism genome-wide association study. *BMC Genomics*. 2012;13(Suppl 8):S16.
130. Valerius MT, Patterson LT, Feng Y, Potter SS. Hoxa 11 is upstream of Integrin alpha8 expression in the developing kidney. *Proc Natl Acad Sci U S A*. 2002;99(12):8090–5.
131. An YJ, Xu WJ, Jin X, Wen H, Kim H, Lee J, et al. Metabotyping of the *C. elegans* sir-2.1 mutant using in vivo labeling and (13)C-heteronuclear multidimensional NMR metabolomics. *ACS Chem Biol*. 2012;7(12):2012–8.
132. Kurtzeborn K, Kwon H, Ihermann-Hella A, Kupari J, Kuure S: Comparative whole-genome transcriptome analysis in renal cell populations reveals high tissue specificity of MAPK/ERK-targets in embryonic kidney GEO <https://www.ncbi.nlm.nih.gov/geo/query/acc.cgi?acc=GSE1742292022>.

Publisher's Note

Springer Nature remains neutral with regard to jurisdictional claims in published maps and institutional affiliations.

Ready to submit your research? Choose BMC and benefit from:

- fast, convenient online submission
- thorough peer review by experienced researchers in your field
- rapid publication on acceptance
- support for research data, including large and complex data types
- gold Open Access which fosters wider collaboration and increased citations
- maximum visibility for your research: over 100M website views per year

At BMC, research is always in progress.

Learn more biomedcentral.com/submissions

